*Journal of Integrative Agriculture 2026, 25(7): 2859–2877*

Available online at ScienceDirect

KeAi CHINESE ROOTS GLOBAL IMPACT

**Journal of Integrative Agriculture**



RESEARCH ARTICLE

# Comparative transcriptome analysis reveals key genes and pathways involved in the development of adventitious roots in tomato

**Hexuan Wang, Xinyi Zhang, Guohao Yang, Xinyi Jia, Jiayi Gao, Haoran Wang, Jingbin Jiang, Jingfu Li, He Zhang, Xiangyang Xu#, Huanhuan Yang#**

*College of Horticulture and Landscape Architecture, Northeast Agricultural University, Harbin 150030, China*

**Highlights**

- Transcriptomic analysis identified the tomato adventitious root induction stage as the key active period.
- Transcriptomic analysis identified the auxin response pathway as the core regulatory dependency for adventitious root initiation.
- The auxin efflux carrier *SlPIN3* positively regulated adventitious root formation *via* mediating polar auxin transport.

**Abstract**

The evolutionary development of adventitious roots (ARs) in plants enhances their capacity to adapt to various stress conditions. A thorough analysis of the influencing factors in their morphological construction holds significant theoretical value and practical guidance for overcoming rooting obstacles in cuttings, as well as for cultivating superior varieties characterized by broad adaptability and stress resistance. In this study, we investigated the molecular mechanisms underlying the development of ARs in tomato (*Solanum lycopersicum*) by performing transcriptome sequencing (RNA-seq). We analyzed the transcription profiles of relevant genes in the "Y962" strain, which exhibits spontaneous AR formation, and the "W961" strain, which does not form ARs. Our findings indicate that the AR induction stage represents an active phase of development, during which we identified 1,676 overlapping genes across the three comparison groups, highlighting the most differentially expressed genes. Functional enrichment analysis showed that they were most closely related to response to auxin, and were also dependent on the crosstalk between other hormones and carbohydrates. Furthermore, through the measurement of endogenous auxin levels and the induction tests with exogenous auxin, it was established that the formation of ARs is closely linked to the accumulation and transport of auxin. Notably, the auxin efflux *SlPIN3*, which was enriched in the auxin response pathway, exhibited significantly high expression during the induction phase of ARs. The *slpin3* mutant, generated using the CRISPR/Cas9 editing system, exhibited a significant reduction in the number of ARs, highlighting the close relationship between polar transport regulated by *SlPIN3* and auxin-induced AR formation. In summary, this study not only enriches the developmental network of AR formation in tomatoes with a wealth of data but also elucidates the potential mechanisms for promoting AR development by targeting *SlPIN3*.

**Keywords:** tomato, adventitious roots, transcriptome, auxin, *SlPIN3*

## 1. Introduction

Crop roots are vital organs that develop within the rhizosphere, serving essential functions such as anchoring crops in the substrate, absorbing water and nutrients, and storing photosynthetic products (Bellini *et al.* 2014; Xie *et al.* 2021). Despite variations among species, nearly all mature crop root systems comprise a primary root, lateral roots (LRs), and adventitious roots (ARs). The primary and lateral roots are categorized under the taproot system, whereas the ARs are classified within the fibrous root system. ARs are defined as roots that develop from existing leaves, stems, old roots, or the hypocotyl of a plant under non-standard conditions

Received 14 April 2025; Received in revised form 10 July 2025; Accepted 9 September 2025; Available online 26 December 2025
Hexuan Wang, E-mail: whxxx36@126.com; #Correspondence Xiangyang Xu, Tel: +86-451-55190214, E-mail: xuxyneau@gmail.com; Huanhuan Yang, Tel: +86-451-55191022, E-mail: huanyaya0126@sina.com

© 2026 CAAS. Publishing services by Elsevier B.V. on behalf of KeAi Communications Co. Ltd. This is an open access article under the CC BY-NC-ND license (http://creativecommons.org/licenses/by-nc-nd/4.0/). Peer review under responsibility of Editorial Board of *Journal of Integrative Agriculture*.
doi: 10.1016/j.jia.2025.12.045

(Franco *et al.* 2011). The formation of ARs can be primarily categorized into two modes: direct formation and indirect formation. For example, in *Poaceae* plants, ARs may form spontaneously, as observed in maize and rice, or may be induced by stress factors, such as flooding and mechanical injury. From an anatomical perspective, ARs can develop from various tissues, including pericycle cells, vascular bundle cells, phloem, or cambium in the stem (Sala *et al.* 2017). The formation of ARs is primarily divided into three stages: induction, initiation, and expression. During the induction stage, cells undergo reprogramming after specialization, acquiring root-forming capabilities. Through cell division and enlargement, the initial cells of the root primordium are formed (Jasik and De Klerk 1997). In the initiation stage, the meristematic cells of the root primordium continue to divide and differentiate, forming an internal structure akin to that of the mature root meristem, which subsequently promotes the emergence of the root primordium (Guan *et al.* 2015). During the expression stage, AR primordia continue to grow and penetrate the epidermal layer, facilitated by programmed cell death, ultimately resulting in the formation of ARs (Lakehal and Bellini 2019). The formation of ARs is a complex organogenetic process regulated by multiple factors, and it is an indispensable biological process in the vegetative reproduction of horticultural crops. Furthermore, this process enhances the adaptability of crops to adverse conditions (Vidoz *et al.* 2010; Calvo-Polanco *et al.* 2012). Therefore, studying the formation of ARs in crops not only aids in understanding the mechanisms of root development but also promotes the widespread application and sustainable development of asexual reproduction techniques for superior varieties. Additionally, this research provides guidance for the selection and breeding of high-quality crop varieties.

The synthesis and metabolic activities of various endogenous plant hormones play a crucial role in the development of ARs (Bai *et al.* 2020). Among these hormones, auxin serves as the primary regulatory hormone for the formation of ARs, exerting precise regulation at different stages of root development through dynamic changes in its concentration (Kevers *et al.* 1997). During the induction phase of ARs, the accumulation of auxin can positively promote the establishment of root primordium cells; however, in the later stages of formation, high concentrations of auxin inhibit the differentiation and elongation of ARs (Ahkami *et al.* 2013). The perception and conduction pathways of auxin signals consist of core components, including Aux/IAA repressor proteins, Transport Inhibitor Response Protein 1 (TIR1), auxin receptor F-box proteins, and transcription factors known as auxin response factors (ARFs). Together, these components mediate the developmental processes of adventitious roots (Dharmasiri *et al.* 2005; Wu *et al.* 2015). The positive regulatory factors TIR1 and AFB2 in ARs form auxin receptor complexes with indole-3-acetic acid (IAA), which inhibit the transcription of *ARF6* and *ARF8*, thereby affecting the expression of GH3 genes and regulating the initiation of ARs (Lakehal *et al.* 2019). In rice, ARF1 protein can bind to the promoter of the downstream *CRL1* gene, inducing its expression and promoting the development of ARs in the lower embryonic axis (Inukai *et al.* 2005). The establishment of a gradient and the asymmetric distribution of auxin are critical throughout the growth and development stages of plants, significantly influencing the overall architecture of plant structures. Auxin is primarily synthesized in the apical meristem of young leaves, stem tips, and root tips, and is subsequently transported to the necessary tissues along the stem *via* intercellular movement (Friml *et al.* 2002; Cheng *et al.* 2007). The polar auxin transport mechanism is primarily facilitated by AUX1/LAX, PIN-FORMED (PIN), and ATP-binding cassette class B (ABCB) transporters (Noh *et al.* 2001; Marhavý *et al.* 2013). The proper functioning of auxin transport proteins is essential for the development of the root system. Specifically, *AUX1* facilitates the influx of auxin into cells, and loss-of-function mutants exhibit a reduced density of LRs. Research indicates that both *aux1* and *lax3* mutants display a phenotype characterized by a decrease in the number of ARs. Furthermore, *AUX1* plays a crucial role in maintaining the balance between the development of vascular tissue in the hypocotyl and the formation of ARs through its expression timing, which occurs earlier than that of *LAX3* (Della Rovere *et al.* 2015). In the ABCB family, the *ABCB19* efflux carrier is predominantly localized in the membranes of endodermal cells within the vascular tissue of *Arabidopsis*. Lines that overexpress this gene exhibit an increased capacity for AR formation, attributed to enhanced auxin transport. Conversely, in *abcb19* knockout mutants, the expression levels of *AtPIN1*, *AtPIN2*, *AtPIN3*, and *AtPIN7* are significantly downregulated, resulting in impaired auxin transport and, consequently, a suppression of AR formation (Sukumar *et al.* 2013). *AtPIN2* regulates cell division, with *pin2* mutant lines displaying shortened roots and reduced sizes of root meristematic tissues (Blilou *et al.* 2005). *AtPIN3* is crucial for the early formation of LRs and plays a dominant role in the gravitropism and phototropism of roots (Ding *et al.* 2011; Rakusová *et al.* 2016). Additionally, *MdPIN7* induces the formation of ARs in apple under the transcriptional regulation of MdARF19 (Wang *et al.* 2024).

Over the years, researchers have identified numerous functional genes that regulate AR development across various plant species. These genes interact with one another to influence the synthesis, transport, and signaling pathways of specific internal factors, thereby playing crucial roles at different stages of AR formation. In rice, OsERF3 protein participates in the initiation of ARs by regulating the expression of *OsRR2*, while the interaction between OsERF3 and OsWOX11 may inhibit *OsRR2* during the elongation process of AR (Zhao *et al.* 2015). AtWOX11, which is homologous to OsWOX11, also binds to the *AtLBD16* promoter, thereby promoting the formation of root primordia *in vitro* during AR development (Liu *et al.* 2018). The expression of *OsCAND1* is restricted to crown roots, and its functional deficiency obstructs the G2/M transition in the meristematic tissue of these roots, thereby inhibiting their normal formation (Wang *et al.* 2011). *OsNAC2* exerts a negative regulatory effect on root growth and the number of crown roots. This effect may be mediated by downregulating the expression of *OsCDK* and *OsCRL* genes, which leads to reduced levels of cytokinins and their signaling (Mao *et al.* 2020). In apples, MdWOX11 directly interacts with the promoter sequence of

*MdLBD29*, thereby promoting the formation of AR primordia, while MdTCP17 downregulates the binding strength of MdWOX11 and *MdLBD29* to their promoters. Furthermore, the protein interaction between MdTCP17 and MdWOX11 reduces the transcriptional activity of *MdLBD29*, thereby indirectly inhibiting the emergence of root primordia (Mao *et al.* 2023). Tomato, as a vine capable of forming ARs spontaneously and inducing root formation under stress, serves as an excellent model for studying the mechanisms of AR development. *SHOOTBORNE ROOTLESS (SBRL/SlLBD17)* may act as a promoting factor during the AR induction stage, regulating both tomato stem rooting and the occurrence of ARs in cuttings (Omary *et al.* 2022). The formation of numerous ARs on the stems of the abscisic acid-deficient mutant *notabilis* is attributed to the loss of function of *LeNCED1*, which encodes 9-*cis*-cyclocarotenoid dioxygenase (Debi *et al.* 2005). Tomato flood-tolerant mutant *rf* causes leaf chlorosis and simultaneously induces abundant AR formation on stems. Researchers have mapped this mutation to the plant porphyrin synthase gene *AUREA* (*AU*), which influences both chlorophyll biosynthesis and the formation of ARs on stems. *AU* plays a crucial role in maintaining hemoglobin homeostasis, facilitating its involvement in AR formation through long-distance transport from leaves to stems (Wu *et al.* 2020).

In this study, we investigated the occurrence process and influencing factors of AR formation in tomato using histological analysis, transcriptome sequencing, endogenous hormone detection, and exogenous hormone treatment. Our results highlighted the significant role of endogenous hormones, particularly auxin, in the AR formation process. Additionally, the accumulation of flavonoids and other related metabolites contributed to the complexity of AR development. Furthermore, we observed that *SlPIN3* was highly expressed during the initial stages of AR formation and actively promoted AR development in tomato.

## 2. Materials and methods

### 2.1. Plant materials and growth conditions

The homozygous inbred lines “W961” (lacking ARs) and “Y962” (possessing ARs), which have been identified across multiple sites for many years, were utilized as experimental materials for transcriptome sequencing and morphological observation. The tomatoes were grown in a growth chamber maintained at a temperature of 25°C, with a photoperiod of 16 hours of light and 8 hours of darkness provided by cold white fluorescent lamps. Tomato plants, 35 days old from seedling, were transplanted into the greenhouse. After 50 days of growth, 10 plants were selected from each of the two materials, and the average number of ARs was counted. The wild-type tomato Ailsa Craig (AC) was selected for genetic transformation. The genetically modified seeds obtained were germinated in the dark and subsequently planted in a growth chamber under a 16 h:8 h light/dark cycle for four weeks prior to phenotype observation and hormone treatment. During this period, standard water and fertilizer management practices, along with appropriate pest control measures, were implemented.

### 2.2. Paraffin section

The anatomical observation focused on stem segments of the “Y962” material, which exhibit varying degrees of AR growth. A stem segment, approximately 0.5 cm in length, was immersed in FAA fixing solution and stored in a refrigerator at 4°C for one day after settling to the bottom of the container. Following this, the stem segments were softened in a 50% glycerol solution for one week and subsequently dehydrated using varying concentrations of ethanol (75%, 85%, 95%, and 100%). After the treatment of stem segments with xylene for transparency, the materials were subsequently embedded in paraffin. The embedded samples were sliced using a Leica rotary microtome (Shanghai, China), and the resulting continuous wax strips were spread and dewaxed. The sections were then stained with saffron and solid green. Finally, the slides were dried and sealed with neutral gum before being observed under an optical microscope.

### 2.3. Sample preparation, mRNA library construction, and sequencing

Based on the morphological changes and anatomical features of the ARs of material ‘Y962’, the sampling was divided into three distinct periods: the AR induction period (where material ‘Y962’ is referred to as ‘BD1’ and material ‘W961’ as ‘MM1’), the AR initiation period (where material ‘Y962’ is referred to as ‘BD2’ and material ‘W961’ as ‘MM2’), and the AR elongation period (where material ‘Y962’ is referred to as ‘BD3’ and material ‘W961’ as ‘MM3’). The stem segments of the plants during these periods were promptly placed in liquid nitrogen at –80°C for subsequent analysis. Each sample of the two materials from each period contains three biological replicates, with each replicate consisting of a mixture of three plants. Total RNA was extracted from the samples using kit A (Thermo Fisher, Waltham, MA, USA). The integrity of the RNA was assessed by agarose gel electrophoresis, while its concentration and purity were measured using an ultraviolet spectrophotometer. Magnetic beads with Oligo (dT) were utilized to enrich mRNA containing polyA tails from total RNA. The isolated RNA was fragmented by interrupting the buffer, followed by reverse transcription using random N6 primers to generate double-stranded DNA. Subsequently, end repair, 5′ end phosphorylation, and 3′ end ligation were performed. PCR amplification was then conducted, resulting in denaturation of the PCR product into single strands. A bridge primer was employed to cyclize the single-stranded DNA, yielding a single-stranded circular DNA library. The constructed library will be sequenced using the DNBSEQ platform (Huada BGI, Shenzhen, China).

### 2.4. Data filtering and gene expression distribution

We utilized the filtering software SOAPnuke (v1.6.2) to eliminate non-standard reads from the raw sequencing data. The resulting clean reads were aligned to the tomato reference genome sequence SL4.0 (ftp://ftp.solgenomics.net/tomato_genome/annotation/ITAG4.0_release) using HISAT (v2.1.0). Bowtie2 was employed to match the clean reads to reference gene sequences, while RSEM was utilized to calculate the gene expression levels for each sample. The

Pearson correlation coefficient was calculated between each pair of samples using R version 4.1.3, based on the expression level data from each sample. Additionally, density plots, box plots, and PCA were generated.

### 2.5. Differentially expressed gene (DEG) analysis and transcription factor family prediction

This study utilized the DESeq2 method, which is based on the principles of the negative binomial distribution, for differential expression analysis. Additionally, the Benjamini-Hochberg method was employed to control the false discovery rate (FDR) for correcting the significance *P*-values. DEGs were identified from various transcriptome comparison combinations, applying thresholds of $\log_2$|fold change (FC)|≥1 and *Q*-value≤0.05. A Venn diagram was generated using R version 4.1.3. The detected open reading frames (ORFs) were compared with transcription factor protein domains using hmmsearch, leading to the prediction and classification of genes with transcription factor-encoding potential based on the family characteristics outlined in PlantTFDB (https://planttfdb.gao-lab.org/).

### 2.6. DEGs cluster analysis and functional analysis

We utilized STEM software to analyze gene expression patterns on the OmicShare platform (www.omicshare.com/tools). Based on the annotations from the Gene Ontology (GO) database and the Kyoto Encyclopedia of Genes and Genomes (KEGG) database, the known DEGs were categorized into GO and KEGG pathways. Enrichment analysis was conducted using the phyper function in R software, with a *Q*-value≤0.05 or *P*-value≤0.05 considered indicative of significant enrichment. Following Signal2Noise sequencing of the gene expression data, Gene Set Enrichment Analysis (GSEA) was performed on the differential genes according to GO database annotations.

### 2.7. Assay of endogenous auxin and induction of exogenous hormone

The internal IAA assay was conducted following the RNA-seq sampling method. Each sample of the two materials from each period contains three biological replicates, with each replicate consisting of a mixture of three plants. The IAA content in plants was quantified using a double antibody one-step sandwich enzyme-linked immunosorbent assay (ELISA). We excised the primary roots of W961, which had grown normally for 20 days post-germination, and transferred the treated plants to a culture container. The control group was treated with clean water, while the treatment groups were supplemented with NAA at concentrations of 0.1, 0.25, and 0.5 μmol $L^{-1}$, or NPA at concentrations of 0.25, 0.5, and 1 μmol $L^{-1}$. Each group consisted of six strains of "W961". The culture medium was changed every two days, and after 6 days of cultivation in a light incubator, the number of ARs was photographed and recorded.

### 2.8. Phylogenetic analysis and subcellular localization

Amino acid sequences of the PIN protein family were downloaded from the SGN (https://solgenomics.net/), TAIR (https://www.arabidopsis.org/) and RAP (https://rapdb.dna.affrc.go.jp/) databases for tomato, *Arabidopsis*, and rice. The MEGA11 software was utilized to construct the phylogenetic tree using the Neighbor-Joining method. The CDS sequence of *SlPIN3*, with the stop codon removed, was incorporated into the linearized pC1300s-GFP vector through homologous recombination. The recombinant plasmid was transformed into the *Agrobacterium* strain GV3101, resulting in the acquisition of *35S::PIN3-GFP*. Following the preparation of the infection solution, tobacco leaves were injected and cultured in the dark for 12 hours before being transferred to standard culture conditions for an additional 48 hours. The fluorescence emission of GFP was observed using a laser confocal microscope (FV3000) (Olympus Corporation, Tokyo, Japan). The primers used in this study are listed in Appendix A.

### 2.9. Construction of gene editing vectors and acquisition of transgenic plants

The CRISPR/Cas9 system was employed to induce mutations in the *SlPIN3* gene. Utilizing the *SlPIN3* sequence information, two target sites were designed using the CRISPR-2.0 P online tool (http://cbi.hzau.edu.cn/CRISP/R2). The sgRNA sequences were synthesized by Genesoul Technology and subsequently inserted into a linearized PV58-K vector to construct the recombinant vector. Following the preparation of the infection solution, the binary vector necessary for genetic transformation was transfected into the WT plants. Leaf DNA from the transgenic plants was extracted for PCR amplification. The types of target mutations were identified through Hi-TOM second-generation sequencing, and homozygous positive plants were subsequently screened. The primers required for vector construction and sequencing are detailed in Appendix A.

### 2.10. Mutant phenotype analysis

The roots of 20-day-old WT and *slpin3* plants were severed and placed in a hydroponic bottle filled with clean water. The water was changed every two days, and the growth of ARs was photographed and documented at two, four, and six days of culture. In the sensitivity experiment of *SlPIN3* to NAA and NPA, WT and *slpin3* plants underwent root cutting and were subsequently transferred to water containing 0.1 μmol $L^{-1}$ NAA or 0.5 μmol $L^{-1}$ NPA, with the culture medium refreshed every two days. After six days of culture, the phenotype was observed, the number of ARs was recorded, and the ARs were collected for Reverse transcription quantitative PCR (RT-qPCR) analysis.

### 2.11. RT-qPCR assay

Total RNA of tomato ARs was extracted by FreeZol Reagent (#R711) Extraction Kit (Vazyme, Nanjing, China). The total RNA was reverse-transcribed into cDNA using HiSIIIRT SuperMix for qPCR (+gDNA wiper) reagent (Vazyme, Nanjing, China). Specific primers were designed by Primer5 and RT-qPCR was performed using SYBR Green reagent. *ACTIN2* was selected as the internal reference gene, and the relative gene expression was calculated by $2^{-\Delta\Delta C_T}$ method. All RT-qPCR analyses were performed with three biological

replicates and three technical replicates. Detailed information about the specific primers is provided in Appendix A.

### 2.12. Statistical analysis of data

Statistical analysis and collation of experimental data were conducted using Microsoft® Excel 2021. A one-way ANOVA was performed on the data using SPSS 23.0 to determine significant relationships among the variables. The results were visualized using histograms plotted with GraphPad Prism 8.

## 3. Results

### 3.1. Phenotypic characteristics of ARs in tomato materials "W961" and "Y962"

Under normal growth conditions, the material "Y962" spontaneously develops a significant number of ARs on the hypocotyl and stem, with their quantity progressively increasing over extended cultivation periods. This phenomenon sharply contrasts with the material "W961," which does not exhibit spontaneous AR formation (Fig. 1-A and B). At 50 days of seedling age, a count of the ARs in both materials revealed a highly significant difference in the average number of ARs (Fig. 1-C). The cross-sectional anatomy of the stem of "Y962" indicates that its primary structure is primarily composed of the epidermis, cortex, and vascular columns, arranged from the outer to the inner layers (Fig. 1-D and E). Notably, some parenchyma cells adjacent to the vascular bundle were densely packed and exhibited a rich cytoplasm, forming distinct small cell clusters that differ from the surrounding cells. These clusters serve as the origin cells for the root primordium (Fig. 1-E). The root primordium originating cells exhibit strong meristematic abilities, continuously dividing and extending towards the epidermis along the direction of the myeloid rays. These cells were closely arranged, with prominent nuclei that appeared almost spherical, characteristic of the AR primordium (Fig. 1-F). As the AR primordium cells continue to divide and differentiate, they become stratified, ultimately completing the establishment of vascular tissue (Fig. 1-G). As the cells gradually elongated, the root cap emerged, and the differentiated primordia of ARs successively penetrated the epidermis and continued to elongate (Fig. 1-H–I). Anatomical observations corroborate the conclusion that the formation of AR roots in tomato can be categorized into three stages: induction, initiation, and expression.

### 3.2. Overall analysis of transcriptome data

This experiment utilized three different stages of two tomato varieties as materials and performed three biological replicates, resulting in a total of 18 samples. Following machine sequencing, each sample yielded an average of 6.34 Gb of data. The filtering process produced at least 39.16 million clean reads. More than 97% of the clean reads exhibited a mass value of ≥20, while values of ≥30 ranged from 92.37% to 94.41%. The average ratio of clean reads to the SL4.0 reference genome sequences was 95.49%, with the proportion of unique mappings to the reference genome varying between 65.53% and 73.86% (Table 1). A total of 26,450 genes were identified, comprising 25,880 known genes and 570 predicted novel genes (Appendix B). The results indicated that the transcriptome data exhibited high base quality and sequencing quality. The correlation

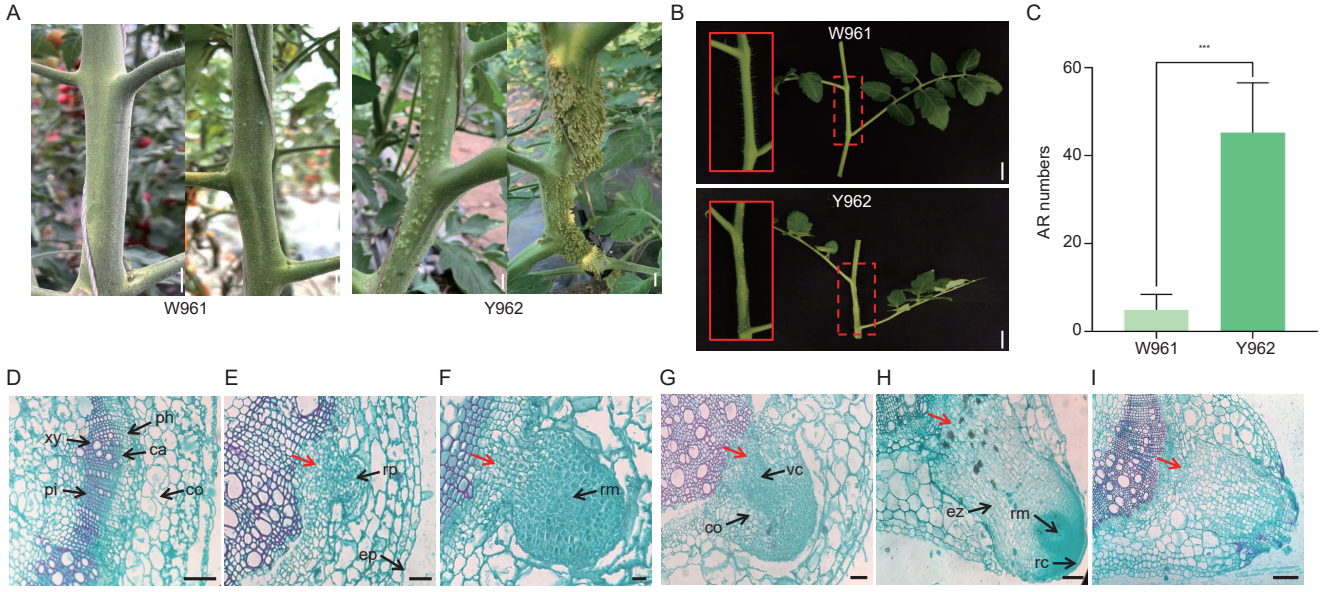



**Fig. 1 Morphological characterization of adventitious roots (ARs) of "W961" and "Y962".** A, the morphology of the ARs of "W961" and "Y962" under normal field conditions. Scale bar=1 cm. B, cauline AR phenotypes at 50 days after seedling emergence. Scale bar=1 cm. C, the number of ARs at 50 days after seedling emergence. Significance was determined by Student's *t*-test ($n$=10). ***, $P$<0.001. D–I, paraffin section of "Y962" stem: initial stem cross section (D), root primordial cell emergence (E), AR formation (F), AR differentiation (G), AR elongation (H), AR breaking through the epidermis (I). ep, epidermis; co, cortex; ca, cambium; ph, phloem; xy, xylem; p, pith; rp, root primordium; rm, root meristem; vc, vascular cylinder; ez, elongation zone; rc, root cap. The red arrows indicate where the root primordium generated. Scale bar=50 μm.

**Table 1 Overview of transcriptome data**

| Sample | Raw reads (M) | Clean reads (M) | Clean bases (Gb) | Q20 (%) | Q30 (%) | Clean reads ratio (%) | Total mapping (%) | Uniquely mapping (%) |
|---|---|---|---|---|---|---|---|---|
| BD1A | 43.82 | 42.45 | 6.37 | 97.62 | 93.8 | 96.86 | 94.58 | 69.73 |
| BD1B | 39.96 | 39.16 | 5.87 | 97.2 | 92.72 | 98.01 | 95.07 | 67.1 |
| BD1C | 41.76 | 41.17 | 6.18 | 97.22 | 92.76 | 98.58 | 95.68 | 67.97 |
| BD2A | 40.99 | 40.34 | 6.05 | 97.25 | 92.84 | 98.41 | 94.98 | 67.65 |
| BD2B | 40.64 | 40.16 | 6.02 | 97.08 | 92.41 | 98.81 | 94.83 | 66.2 |
| BD2C | 42.61 | 41.96 | 6.29 | 97.09 | 92.46 | 98.48 | 95.34 | 65.53 |
| BD3A | 43.82 | 43.08 | 6.46 | 97.06 | 92.37 | 98.3 | 95.37 | 66.16 |
| BD3B | 43.82 | 43.19 | 6.48 | 97.16 | 92.62 | 98.56 | 94.92 | 66.92 |
| BD3C | 43.82 | 42.82 | 6.42 | 97.66 | 93.8 | 97.72 | 95.09 | 69.89 |
| MM1A | 43.82 | 42.99 | 6.45 | 97.91 | 94.41 | 98.11 | 96.17 | 73.86 |
| MM1B | 43.82 | 43.08 | 6.46 | 97.57 | 93.57 | 98.31 | 95.53 | 70.51 |
| MM1C | 43.82 | 43.08 | 6.46 | 97.58 | 93.59 | 98.3 | 96.04 | 71.54 |
| MM2A | 43.82 | 43.17 | 6.48 | 97.41 | 93.13 | 98.52 | 96.17 | 69.59 |
| MM2B | 43.82 | 42.85 | 6.43 | 97.26 | 92.77 | 97.78 | 95.33 | 67.04 |
| MM2C | 43.82 | 42.99 | 6.45 | 97.56 | 93.56 | 98.09 | 96.04 | 70.87 |
| MM3A | 43.82 | 43.15 | 6.47 | 97.59 | 93.61 | 98.46 | 96.04 | 71.98 |
| MM3B | 43.82 | 42.69 | 6.4 | 97.76 | 94.02 | 97.43 | 95.79 | 72.54 |
| MM3C | 43.82 | 43.16 | 6.47 | 97.63 | 93.71 | 98.48 | 95.89 | 71.71 |

coefficient of samples across the three periods of “Y962” was consistently higher than that of “W961”, indicating that the expression levels among the three biological replicates were similar and more reliable (Fig. 2-A). After data normalization, the density map and box plot illustrated that the expression data in each group was evenly distributed, with moderate FPKM values (Fig. 2-B and C). The dispersion of the data was further analyzed using principal component analysis (PCA), revealing that PC1 and PC2 accounted for 69.59% and 11.74% of the variation, respectively. Notably, the BD1 samples exhibited the highest degree of separation in both PC1 and PC2, suggesting that the AR induction period represented by BD1 was a critical phase (Fig. 2-D).

### 3.3. Statistical analysis and transcription factors (TFs) identification of DEGs

Based on the gene expression levels of each sample, a total of 24,569 DEGs were identified across nine groups (Fig. 3-A). Among these, 2,570 DEGs were up-regulated and 2,595 DEGs were down-regulated in the comparison of BD1 *vs.* BD2. In the comparison of BD1 *vs.* BD3, a total of 3,853 up-regulated DEGs and 3,850 down-regulated DEGs were detected. The comparison of BD2 *vs.* BD3 revealed 1,284 up-regulated DEGs and 915 down-regulated DEGs. Additionally, a total of 2,770 DEGs were identified in the pairings of MM1, MM2, and MM3, which accounts for 11.2% of the total DEGs. When comparing MM1 with BD1, MM2 with BD2, and MM3 with BD3, the following numbers of up-regulated genes were identified: 2,460, 1,264, and 503, respectively, while the down-regulated genes were 2,268, 620, and 237, respectively. In the case of comparing the same materials across three different periods, the DEGs identified in material “Y962” were significantly more numerous than those in material “W961”. This finding suggested a greater presence of genes associated with AR development in “Y962”. The number of DEGs detected in BD1-vs-BD2 is greater than that in BD2-vs-BD3. Notably, the comparison group that yielded the highest number of DEGs from both materials was MM1-vs-BD1. These findings suggested that gene expression was more vigorous during the transition from the induction of adventitious roots to the initiation of root primordium differentiation, as opposed to the phase of AR elongation until it penetrated the epidermis.

When the screening criteria were established with a $\log_2|\text{fold change (FC)}|\geq 1$ and a *Q*-value of≤0.05, three comparison groups exhibiting a higher number of DEGs between the two varieties were selected to create a Venn diagram (Fig. 3-B). The results indicated that a total of 1,676 genes were significantly different across the comparisons of BD1-vs-BD2, BD1-vs-BD3, and MM1-vs-BD1, suggesting that these genes are likely to play a key role in mediating the occurrence of ARs (Appendix C). Additionally, multiple transcription factor families have been reported to regulate AR formation in crops. Through the analysis of 1,676 DEGs, we identified 112 TFs, categorized into 25 distinct families. Among these, the significantly enriched families primarily include bHLH, MYB, WRKY, NAC, AP2-EREBP, and LOB (Fig. 3-C). By presenting their expression levels in the form of heat maps, we observed that the TFs from the bHLH and MYB families were predominantly expressed during the BD1 stage. In contrast, the TFs from the WRKY and NAC families exhibited high expression levels during the BD2 or BD3 stages, with the expression level of MM1 also surpassing that of BD1 at the same stage (Fig. 3-D; Appendix D). These results indicated that different members of distinct TF families play specific regulatory roles at various stages of AR development.

### 3.4. DEGs expression at different developmental stages of ARs

By clustering the expression levels of FPKM at various stages of AR development (BD1, BD2, BD3), we categorized the 1,676 identified overlapping DEGs into eight distinct trends (Fig. 4-A). Genes within the same group exhibit identical

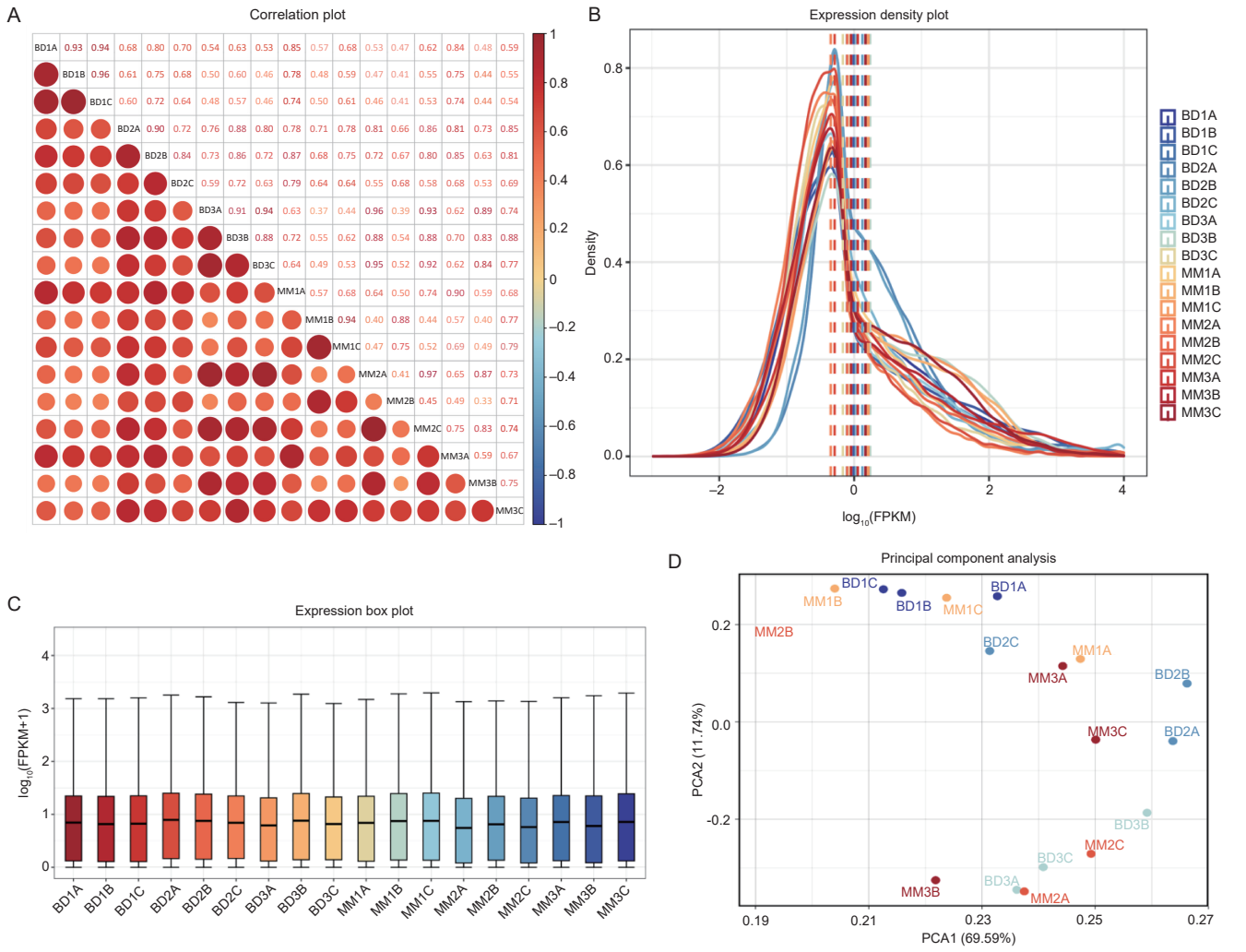



**Fig. 2 Overview of RNA-seq data.** A, correlation heat maps for 18 samples. The *X* and *Y* axes represent each sample, with the values indicating the correlation coefficients. The intensity of the red color reflects the degree of correlation: darker shades signify higher correlations, while lighter shades indicate lower correlations. B, density plot of FPKM. C, expression box plot. The expression box plot for each region presents five statistics: upper quartile, median quartile, lower quartile, and lower limit, arranged from top to bottom (the upper and lower limits do not account for outliers). D, principal component analysis (PCA).

expression patterns, suggesting that they may fulfill specific functions related to AR occurrence at corresponding stages. Our results indicated that four profiles (0, 1, 6, and 7) were significantly enriched trend sets. Notably, profile 6 contained the largest number of DEGs, totaling 587, and exhibited an expression pattern characterized by an initial increase followed by a plateau (Appendix E). Conversely, the module with the most significant enrichment was profile 0, where the expression trend consistently declined throughout the AR formation process (Fig. 4-A). We subsequently analyzed the KEGG pathways of the three most significantly enriched trend sets (Fig. 4-B and C; Appendix F). The 458 differential genes identified in profile 0 were primarily concentrated in two pathways: 'starch and sucrose metabolism' and 'plant hormone signal transduction'. Additionally, these genes were involved in several metabolic pathways, including 'arginine biosynthesis', 'phenylpropanoid biosynthesis', 'cyanoamino acid metabolism', 'fatty acid elongation', and 'RNA polymerase'. In contrast, the gene enrichment terms for profile 6 encompassed 'plant-pathogen interaction', 'MAPK signaling pathway-plant', 'flavonoid biosynthesis', 'arachidonic acid metabolism', along with five other biosynthetic pathways. The pathway with the most significant and enriched genes in profile 1 was plant hormone signal transduction. Additionally, DEGs have been identified in other biosynthetic degradation pathways, including the degradation of valine, leucine, and isoleucine, as well as circadian rhythm regulation in plants. These findings suggested that relevant hormones played a predominant role in inducing ARs during their growth and development. Furthermore, various biosynthetic and degradation metabolic processes were highly active, indicating that the occurrence of ARs was associated with intense cellular activity, which necessitated the continuous synthesis and degradation of large molecules to maintain stability and obtain energy.

### 3.5. GO and GSEA enrichment analysis of DEGs

To enhance our understanding of the relevant functions of DEGs, we performed GO classification and enrichment

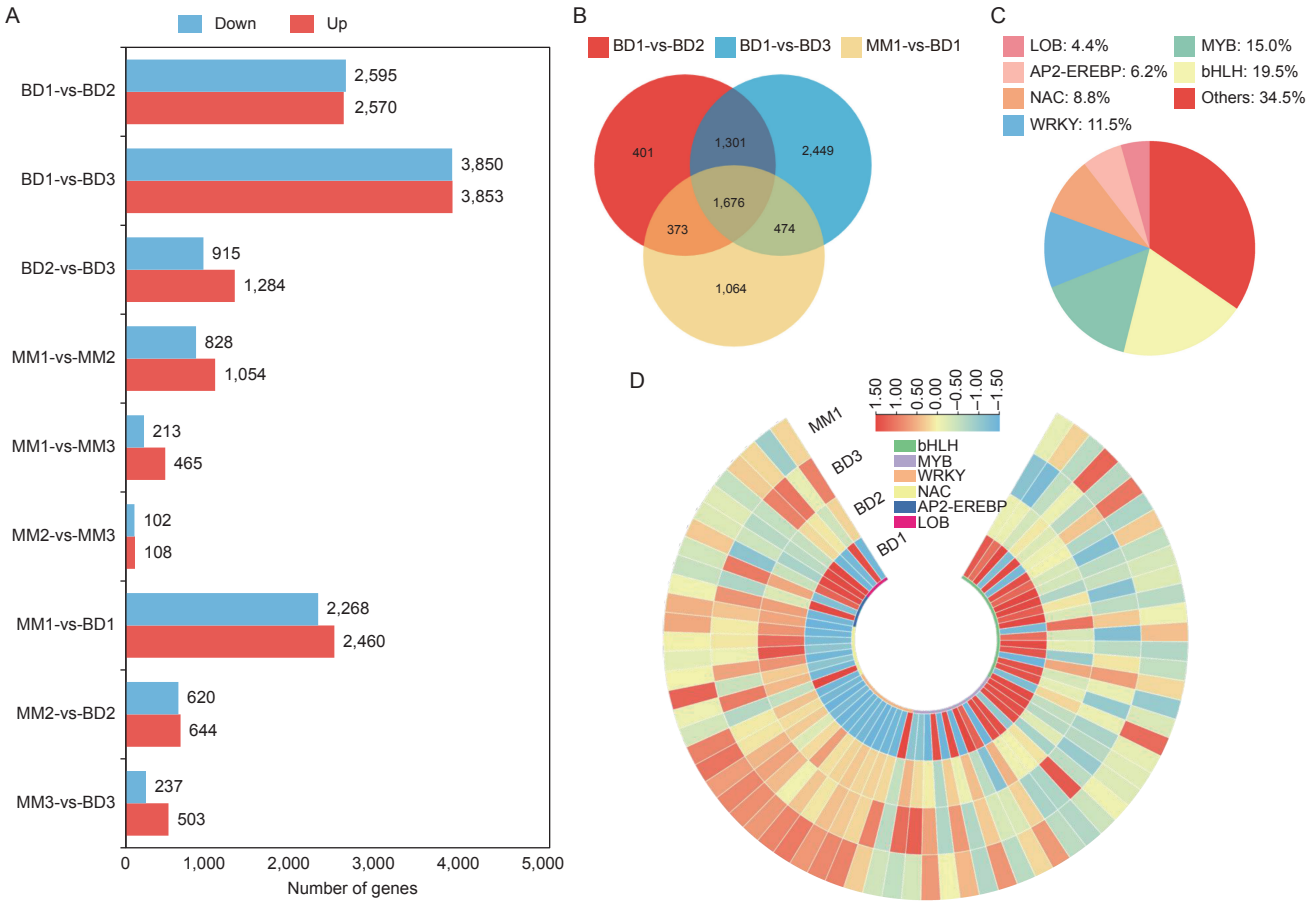
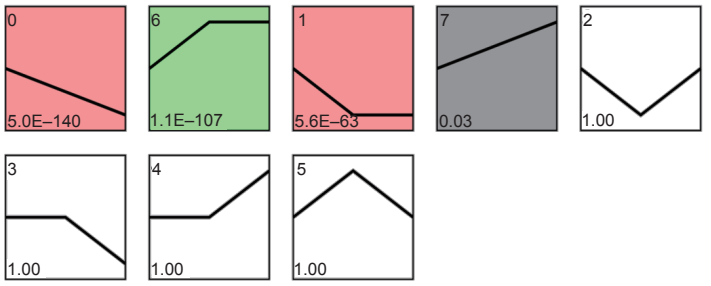



**Fig. 3 Screening of differentially expressed genes (DEGs) and identification of transcription factors (TFs) across different groups.** A, statistical analysis of differentially expressed genes. The *Y*-axis represents the comparison scheme for each group, while the *X*-axis displays the corresponding number of DEGs. Red indicates the number of up-regulated DEGs, and blue indicates the number of down-regulated DEGs. B, venn diagrams illustrating the differential genes among the comparison groups BD1-vs-BD2, BD1-vs-BD3, and MM1-vs-BD1. C, pie charts depicting the 1,676 TF families associated with DEGs. D, heatmap expression profiles of significantly enriched TFs.

analysis on DEGs common to the three comparison groups. As illustrated in Fig. 5-A, among the 1,676 overlapping DEGs identified in biological processes, the most prevalent GO terms were 'cellular process' and 'metabolic process'. In the cellular component category, 'cellular anatomical entity' encompassed the highest number of differential genes, followed closely by numerous 'intracellular' terms. Regarding molecular function, the prominent GO terms identified were 'binding' and 'catalytic activity.' The GO functional classification indicates that DEGs in ARs are primarily associated with cellular metabolism, binding, and catalytic processes. Furthermore, the GO enrichment analysis of the overlapping DEGs revealed that 72 functional pathways were significantly enriched ($Q$-value≤0.05). The first 20 enrichment pathways were selected for further study, revealing that DEGs primarily focused on biological processes, particularly in two key areas: hormones and growth (Fig. 5-B; Appendix G). The pathways associated with hormones included 'response to auxin', 'response to hormone', 'auxin polar transport', 'auxin transport', and 'hormone transport'. In contrast, the pathways related to growth encompassed 'regulation of developmental growth', 'regulation of growth', and 'regulation of organic growth'. These findings indicated that the growth and development of ARs were closely linked to the transport and regulation of endogenous hormones, with a particular emphasis on auxin. Regarding cellular components, the pathways related to the 'cell periphery', 'plasma membrane', and 'intrinsic component of plasma membrane' were notably concentrated, indicating that the formation of ARs necessitates the cell membrane's role in maintaining intracellular stability and facilitating material exchange.

To investigate the association between functional gene sets and AR genesis, we first standardized the gene expression data and subsequently performed GSEA utilizing the GO database for the comparisons BD1-vs-BD2, BD1-vs-BD3, and MM1-vs-BD1. Based on the enrichment score (ES), we ranked the associations between the results and phenotypes. By integrating the GO enrichment results of the 1,676 overlapping DEGs mentioned previously, we ultimately selected the auxin response pathway for in-depth study. This pathway is notably highly expressed and demonstrates significant performance during the BD1 stage (Fig. 5-D–F). A total of 35 auxin-related differential genes were enriched in this pathway, all of which are implicated as core genes in the formation of ARs (Appendix H). We identified the intersection of fifty-five genes directly enriched by GO in the context of 'response to auxin' and 35 genes enriched by GESA, resulting in 31 common auxin-

A




B

| Pathway name (KEGG) | profile0 | profile6 | profile1 |
|---|---|---|---|
| Starch and sucrose metabolism | 1.37E–05 | | 4.81E–02 |
| Plant hormone signal transduction | 2.23E–04 | | 9.76E–04 |
| Arginine biosynthesis | 1.85E–02 | | |
| Phenylpropanoid biosynthesis | 1.96E–02 | | |
| Cyanoamino acid metabolism | 2.07E–02 | | |
| Fatty acid elongation | 2.35E–02 | | |
| RNA polymerase | 3.08E–02 | | |
| Plant-pathogen interaction | | 4.11E–06 | |
| MAPK signaling pathway-plant | | 6.88E–05 | |
| Flavonoid biosynthesis | | 1.56E–04 | |
| Arachidonic acid metabolism | | 6.11E–04 | |
| Isoflavonoid biosynthesis | | 1.70E–03 | |
| Flavone and flavonol biosynthesis | | 9.29E–03 | |
| Benzoxazinoid biosynthesis | | 3.83E–02 | |
| Brassinosteroid biosynthesis | | 4.40E–02 | |
| RNA degradation | | 4.95E–02 | |
| Valine, leucine and isoleucine degradation | | | 1.03E–03 |
| Circadian rhythm-plant | | | 2.01E–03 |
| Sphingolipid metabolism | | | 2.05E–03 |
| Glycosphingolipid biosynthesis-ganglio series | | | 8.06E–03 |
| Betalain biosynthesis | | | 1.94E–02 |
| Glycosaminoglycan degradation | | | 2.34E–02 |
| Other glycan degradation | | | 3.08E–02 |
| Glycerolipid metabolism | | | 3.41E–02 |
| Steroid biosynthesis | | | 3.51E–02 |
| Glycerophospholipid metabolism | | | 4.56E–02 |

C

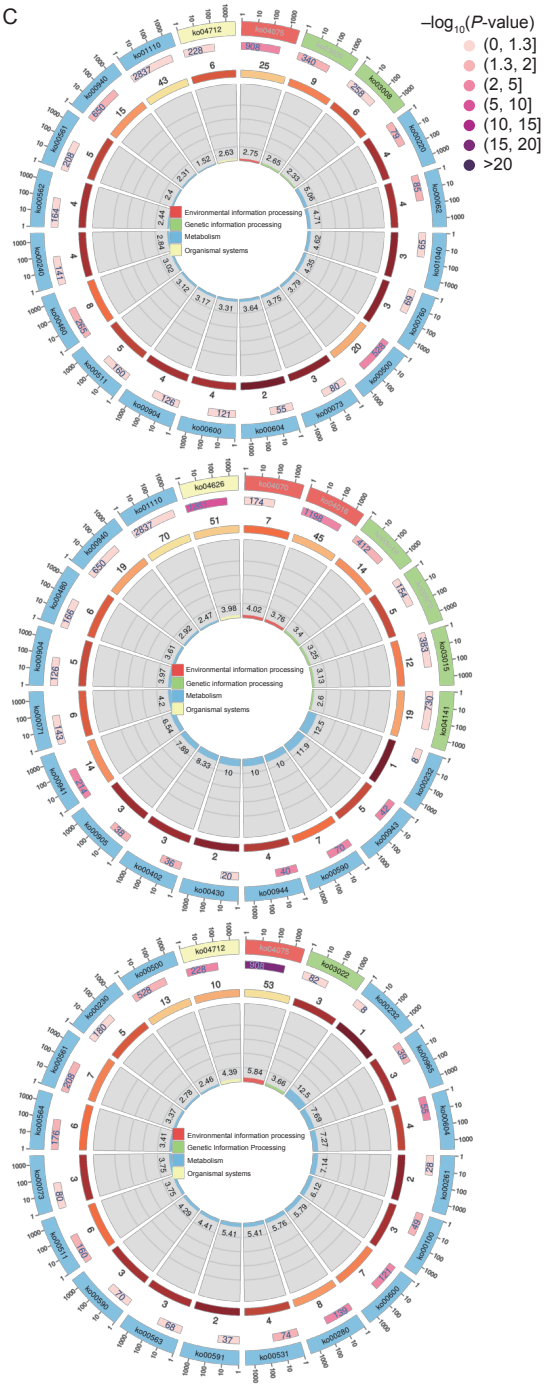



**Fig. 4 Gene expression patterns and functional transition at different adventitious root (AR) development stages.** A, *P*-values are provided for each trend module. The colored trend block indicates significant enrichment, while the uncolored trend block signifies non-significant enrichment. B, KEGG analysis revealed that genes in profiles 0, 6, and 1 were significantly enriched (*P*-value<0.05). C, the KEGG enrichment circles for genes in profiles 0, 6, and 1 illustrate the following: the first circle displays the top 20 enriched pathway classes, the second circle indicates the number of genes in the background, the third circle represents the number of differential genes within each pathway, and the fourth circle shows the rich factor value for each pathway.

related genes. We visualized their expression levels using heatmaps (Fig. 5-C). The identified genes predominantly included ‘auxin-responsive protein IAA’, ‘small auxin up-regulated RNA’, and ‘auxin efflux facilitator’. Notably, their expression was the highest in BD1 and decreased with the continuous formation of ARs. Furthermore, the expression levels of auxin-related genes in “W961 “were significantly lower than those observed in “Y962”. These findings suggested that auxin was enriched at a specific developmental stage, actively contributing to AR induction.

### 3.6. Expression patterns of related genes mediating AR development

Based on a comprehensive analysis and screening of 1,676

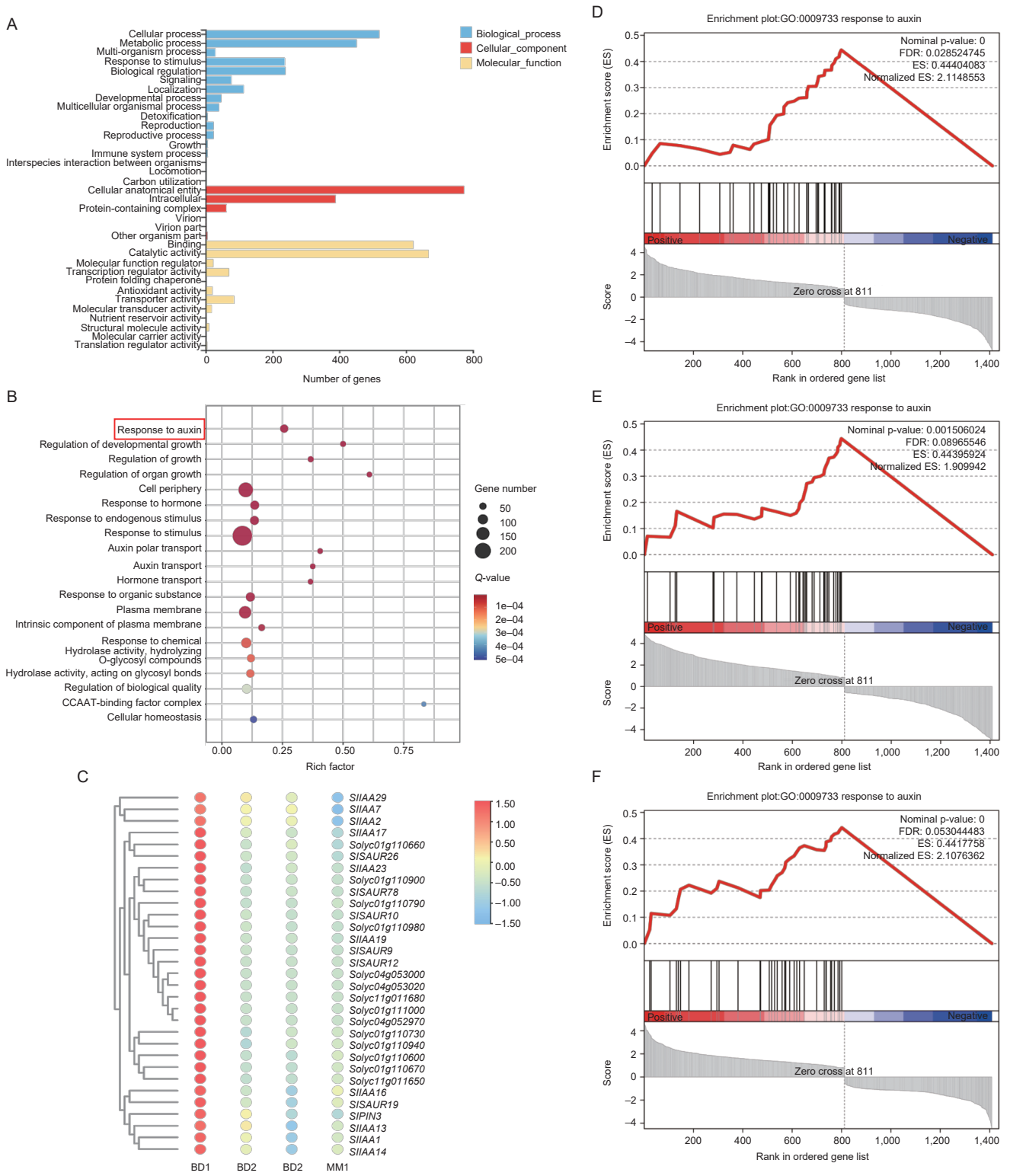



**Fig. 5 Functional classification and enrichment analysis of differentially expressed genes (DEGs).** A, GO classification of 1,676 overlapping DEGs. The *X*-axis represents the number of genes annotated to GO entries, while the *Y*-axis denotes the functional classification within GO. B, enrichment bubble plot for the 1,676 overlapping DEGs related to GO. The *X*-axis indicates the enrichment ratio, the *Y*-axis represents the GO term, the size of the bubbles reflects the number of DEGs annotated to a specific GO term, and the color denotes the enrichment *Q*-value. C, a heatmap illustrating the expression levels of the 1,676 overlapping DEGs enriched in GO and GSEA in response to the auxin pathway. D–F, the GSEA-GO enrichment map for the auxin response pathway corresponds to three comparison groups: BD2-vs-BD1, BD3-vs-BD1, and MM1-vs-BD1.

genes that were differentially expressed in the BD1-vs-BD2, BD1-vs-BD3, and MM1-vs-BD1 comparison groups, we proposed that a total of 61 DEGs might be involved in the development of ARs (Fig. 6-A; Appendix I). There are two

types of receptors involved in auxin signal transduction: TIR1/AFBs and AUX/IAAs. We identified a total of nine auxin-responsive genes (*SlIAA16*, *SlIAA19*, *SlIAA17*, *SlIAA7*, *SlIAA2*, *SlIAA29*, *SlIAA1*, *SlIAA14*, and *SlIAA13*). The polar transport of auxin necessitates the mediation of three transporters (AUX/LAX, ABCB, and PIN). In this experiment, we identified two influx carriers (*SlLAX4* and *SlLAX3*) and one efflux carrier (*SlPIN3*). Additionally, we discovered auxin early response genes, including six SAURs and one GH3-like gene. Auxin-related genes exhibited high expression levels during the AR induction period. During the differentiation and elongation stages, the expression levels of most of these genes continued to decline, while some remained stable or increased. Cytokinin is another hormone that plays a crucial role in the growth and development of ARs, sometimes acting antagonistically to auxin. We identified four two-component response regulators; with the exception of ARR-B, which exhibited the highest expression level during AR extension, the expression levels of *LePCL1*, *ARR3*, and *ARR9* gradually decreased as ARs formed. Additionally, the expression levels of three cytochrome riboside 5′-monophosphate phosphoribohydrolase genes (*LOG8*, *LOG3*, and *LOG6*) were also downregulated. The gene encoding the gibberellin receptor (*GID1*) and the scarecrow protein 14 gene (*SCL14*) exhibited peak expression levels during AR extension. In contrast, the genes encoding gibberellin oxidase (*GA2ox8*, *SlGA3ox2*, *GA2ox4*) and gibberellin-regulated proteins (*GRP14* and *GPL6*) displayed high activity during AR induction. The peak expression of the abscisic acid receptor (*PYL4-like*, *PYL1* and *PYL6*) was observed during the

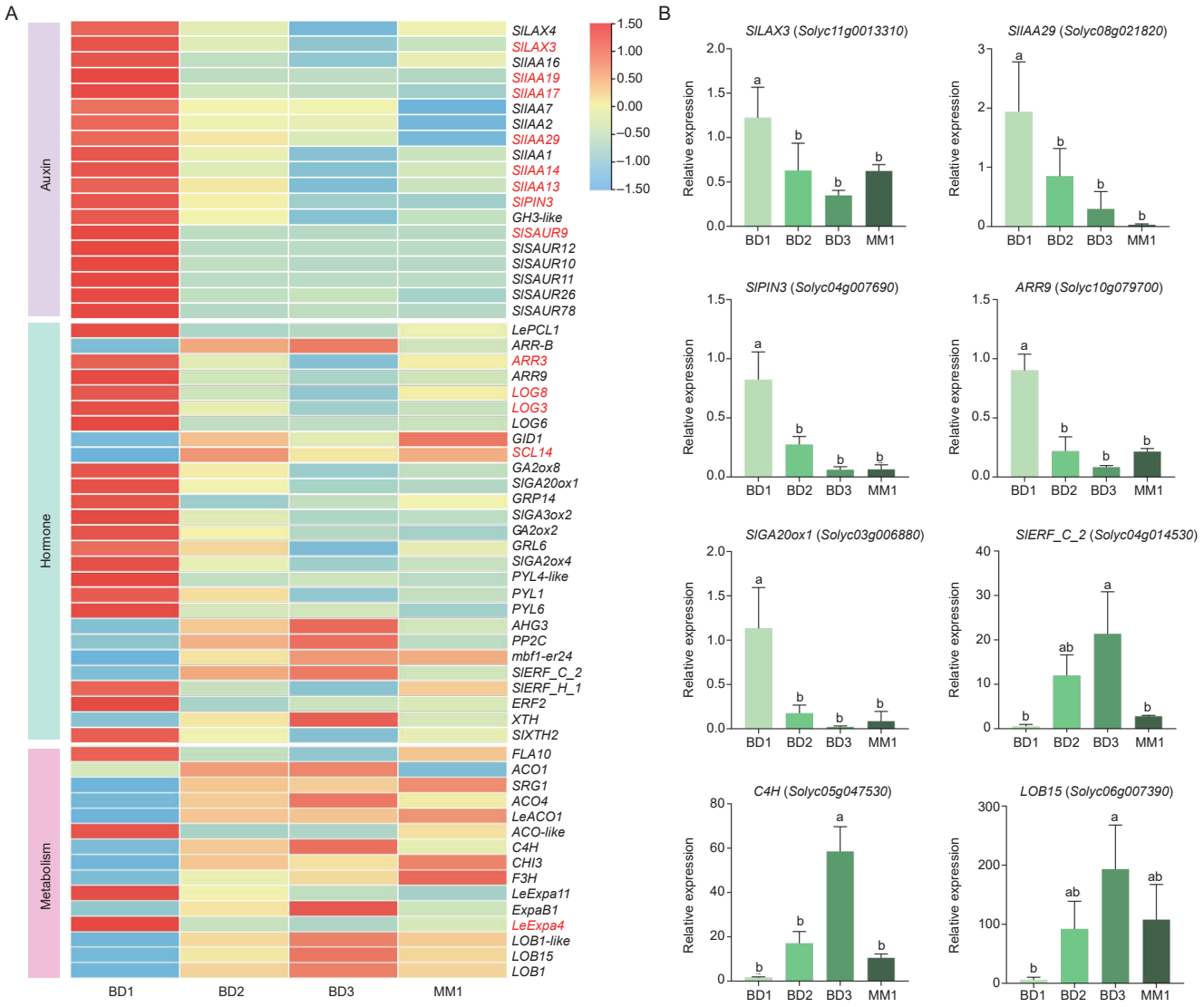



**Fig. 6 Expression profiles of differentially expressed genes (DEGs) that may be involved in the occurrence of adventitious roots (ARs) and RT-qPCR validations of RNA-seq data.** A, expression calorimetry of potential target genes regulating AR formation among 1,676 overlapping differential genes identified through RNA-seq analysis. The genes marked in red represent relevant literature references. The bold font is the gene detected by RT-qPCR in the right figure. B, the expression profiles of eight differentially expressed genes were verified using RT-qPCR, with three biological replicates and three technical replicates conducted for each sample. One-way ANOVA was employed to analyze significance. Different lowercase letters indicate significant differences between groups at the $P<0.05$ level, while the same lowercase letters indicate no significant differences between groups.

induction phase, whereas Protein Phosphatase 2C (*AHG3* and *PP2C*) was induced during the elongation phase. Four genes involved in ethylene signaling — *mbf1-er24* and *SlERF_C2* — demonstrated increased expression levels compared to the induction period, while *SlERFH_1* and *ERF2* showed decreased expression levels. The expression trends of two genes encoding xyloglucan endotransglucosylase/hydrolase in the brassinosteroid pathway were observed to be oppositional. The metabolic activity of carbohydrates, which is regulated by hormones, serves as the energy source for the entire process of AR development, which in turn can stimulate hormones to exert their biological effects. The gene *FLA10*, associated with sucrose and starch metabolism, may play a role in the early stages of AR formation. The expression levels of genes involved in the flavonoid synthesis pathway (*ACO1*, *LeACO1*, *C4H*, *CHI3*, etc.) varied. Expansin proteins facilitate cell wall relaxation by mediating pH-dependent extension and promoting cell growth, thereby promoting cell expansion. In our study, we identified three expansion proteins. Notably, the expression level of *ExpaB1* continuously increased, whereas the expression levels of *LeExpa11* and *LeExpa14* exhibited a downward trend. For the genes preferentially expressed in AR induction stage, the expression of "Y962" was higher than that of "W961". Conversely, genes that were less active during this induction period demonstrate elevated expression levels in "W961" relative to "Y962". To verify the reliability of the RNA-seq results, we randomly selected eight DEGs from those that may regulate the growth and development of ARs for RT-qPCR validation. The results indicated that the RT-qPCR findings were consistent with the transcriptome data, thereby further confirming the reliability of the RNA-seq data (Fig. 6-B).

### 3.7. Induction of ARs in tomato by auxin

Auxin has been established as the primary inducer of AR development in previous studies. In this experiment, an analysis of transcriptomic data revealed that the DEGs in the materials W961 and Y962 were enriched in the auxin response pathway. To further investigate the expression pattern of auxin during AR development, we measured the indole-3-acetic acid (IAA) content in ARs of various materials at different stages. The results indicated that the endogenous IAA content in "Y962" was significantly higher than that in "W961" at the initial stage of AR formation (Fig. 7-A). Additionally, IAA content gradually decreased from the induced differentiation stage to the point of breaking through the epidermis, suggesting that auxin may facilitate the induction of ARs while inhibiting their elongation. Furthermore, we conducted exogenous auxin induction experiments on "W961" to explore the effects of auxin on ARs more comprehensively (Fig. 7-C and E).

The results indicated that the application of 0.1 and 0.25 μmol $L^{-1}$ NAA stimulated the production of ARs, resulting in an increase in the number of roots by 1.26 and 0.93 times, respectively, compared to the control group. However, in the presence of 0.5 μmol $L^{-1}$ NAA, the number of ARs generated was lower than that observed in the control group. While NAA at appropriate concentrations promoted adventitious root formation, it significantly restricted root length (Fig. 7-B and E). Similarly, our findings demonstrated that the exogenous application of varying concentrations of NPA inhibited AR formation in tomatoes, with 0.5 μmol $L^{-1}$ NPA exhibiting the most pronounced inhibitory effect (Fig. 7-D and E). These results suggest that low concentrations of auxin facilitate the initiation of ARs, whereas the inhibition of auxin transport obstructs AR development.

### 3.8. *SlPIN3* is a candidate gene for regulating ARs

To further investigate the relationship between auxin and AR development, we selected appropriate genes for functional validation based on the conclusions drawn from transcriptome analysis and previous research findings. The PIN protein family is a well-established auxin export carrier that plays a crucial role in the transport and distribution of auxin, thereby assisting in the regulation of plant growth and development mediated by auxin. Based on previous research, we have found that multiple PIN family genes are related to the growth and development of plant root systems (Xu *et al.* 2005; Hu *et al.* 2023). In this study, *SlPIN3* was the only gene identified among the 1,676 DEGs. The expression levels of other PIN family genes did not exhibit significant differences and were largely non-expressive. Meanwhile, both RNA-seq and RT-qPCR results demonstrated that *SlPIN3* was preferentially expressed during the AR induction stage and was down-regulated during the formative stage. GO functional enrichment and GSEA results indicate that *SlPIN3* was enriched in auxin response pathways, suggesting it is likely a core gene regulating traits associated with ARs. Consequently, we have selected *SlPIN3* as a candidate target gene for studying the pathogenesis of ARs. Tomatoes contain a total of 10 PIN proteins (SlPIN1 to SlPIN10). To elucidate their evolutionary relationships with other species, we constructed phylogenetic trees for tomato, *Arabidopsis* and rice (Fig. 8-A). The phylogenetic analysis revealed that the proteins SlPIN3 and SlPIN4 share a branch with AtPIN3, AtPIN4, and AtPIN7, indicating a closely related evolutionary origin. The subcellular localization of SlPIN3 was observed on the cell membrane, aligning with the established conclusion that PIN proteins are membrane proteins (Fig. 8-B). In conclusion, based on the phylogenetic analysis of SlPIN3 protein, it was reasonable to infer that it possessed similar physiological functions to its homologous genes in *Arabidopsis thaliana* during AR development.

### 3.9. *SlPIN3* promotes the occurrence of ARs

We constructed a mutant of *SlPIN3* using the CRISPR/Cas9 system to further investigate its effects on ARs. Two different target sites were identified within the first exon region of *SlPIN3* and integrated into the CRISPR/Cas9 vector. Sequencing analysis revealed that *slpin3-c1* inserted a base at the first target site while exhibiting a base deletion at the second target site, resulting in a frameshift mutation. Similarly, *slpin3-c2* displayed a base deletion at the first target site, leading to a frameshift in the open reading frame and premature termination of translation (Fig. 9-A). Furthermore, the expression levels of *SlPIN3* in these two mutant systems

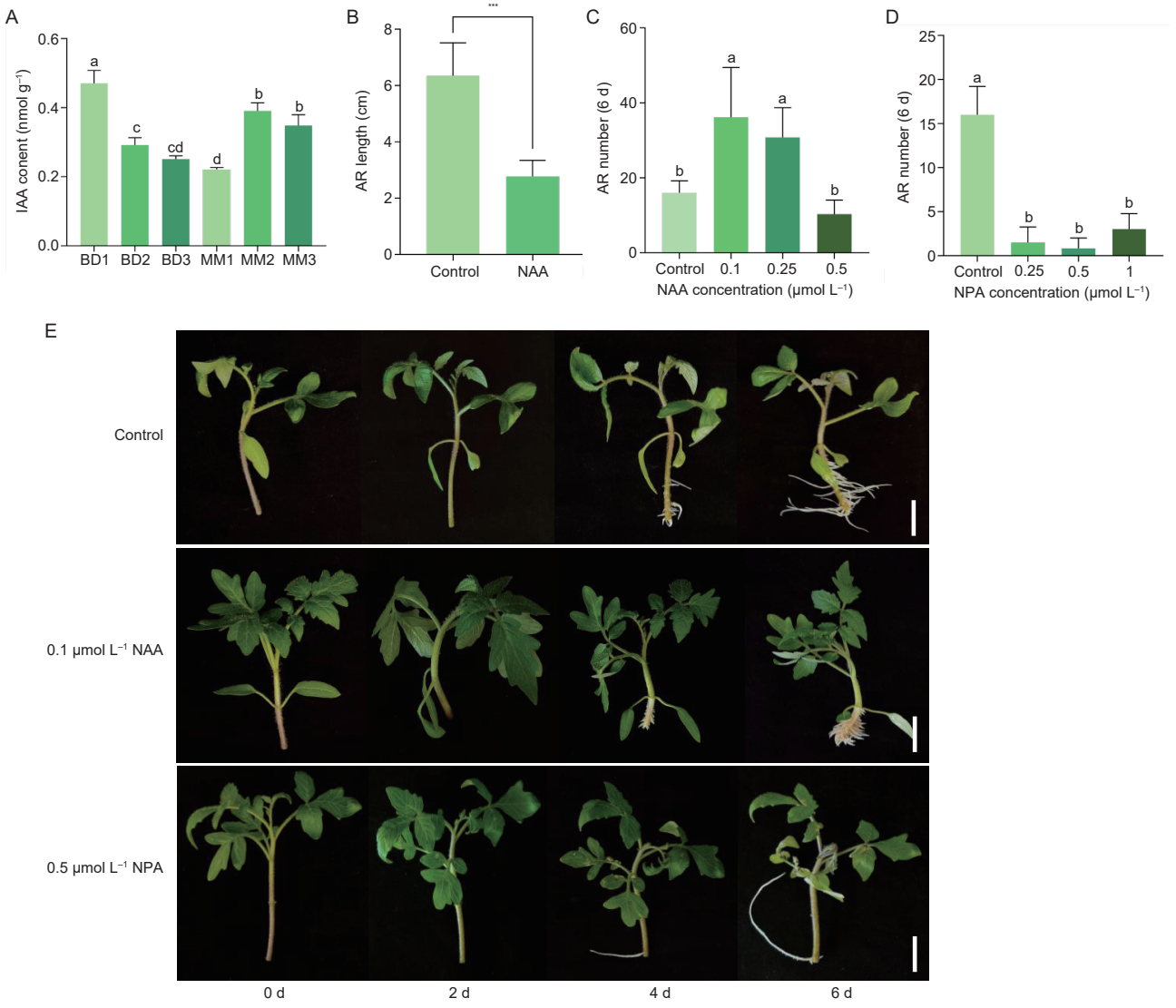



**Fig. 7 Determination of endogenous indole-3-acetic acid (IAA) content and effects of exogenous hormone application on adventitious roots (ARs).** A, changes in endogenous IAA content during various stages of AR formation in "W961" and "Y962". B, the length of ARs under control and NAA treatment. C and D, the number of ARs formed by "W961" under control conditions and following treatment with different concentrations of NAA (0.1, 0.25, 0.5 μmol $L^{-1}$) or NPA (0.25, 0.5, 1 μmol $L^{-1}$) is presented. Values are expressed as mean±SE (*n*=6). Significance analysis was conducted using Student's *t*-test or one-way ANOVA, with ***, *P*<0.001. Different lowercase letters indicate significant differences between groups at the *P*<0.05 level, while the same lowercase letters indicate no significant differences between groups. E, representative images of tomato ARs after exogenous application of 0.1 μmol $L^{-1}$ NAA and 0.5 μmol $L^{-1}$ NPA. Scale bar=1 cm.

were significantly lower than those in the WT (Fig. 9-C), indicating a loss of function. Consequently, we selected the offspring of these two homozygous mutant strains for subsequent research.

After four days of culture, ARs appeared at the stem incision of both WT and *slpin3* mutant plants. However, the number of ARs was greater in the WT. In the WT, the ARs had penetrated the epidermis, whereas in the *slpin3* mutant, the ARs were only slightly convex (Fig. 9-B and D). The development of ARs in the *slpin3* was slower compared to that in WT plants. By the sixth day, the ARs exhibited continued growth, with the number generated by the WT significantly surpassing that of the *slpin3* mutant plants (Fig. 9-B and D). To assess whether *SlPIN3* mutations affect polar auxin transport, both WT and mutants, at 20 days of seedling age, were treated with 0.1 μmol $L^{-1}$ NAA and 0.5 μmol $L^{-1}$ NPA solutions. Experimental results indicate that, regardless of the treatment applied, the knockout of the *SlPIN3* gene significantly inhibited the formation of ARs (Fig. 10-A). In a 0.1 μmol $L^{-1}$ NAA solution, the number of ARs produced by the WT on day 6 was 1.87 times and 2.02 times greater than that of the *slpin3-c1* and *slpin3-c2* mutants, respectively. In a 0.5 μmol $L^{-1}$ NPA solution, the number of ARs produced by both the mutant and WT decreased by 63.3 and 55.1%, respectively, on the sixth day (Fig. 10-C). For *slpin3-c1* and *slpin3-c2*, the number of ARs generated under NAA treatment

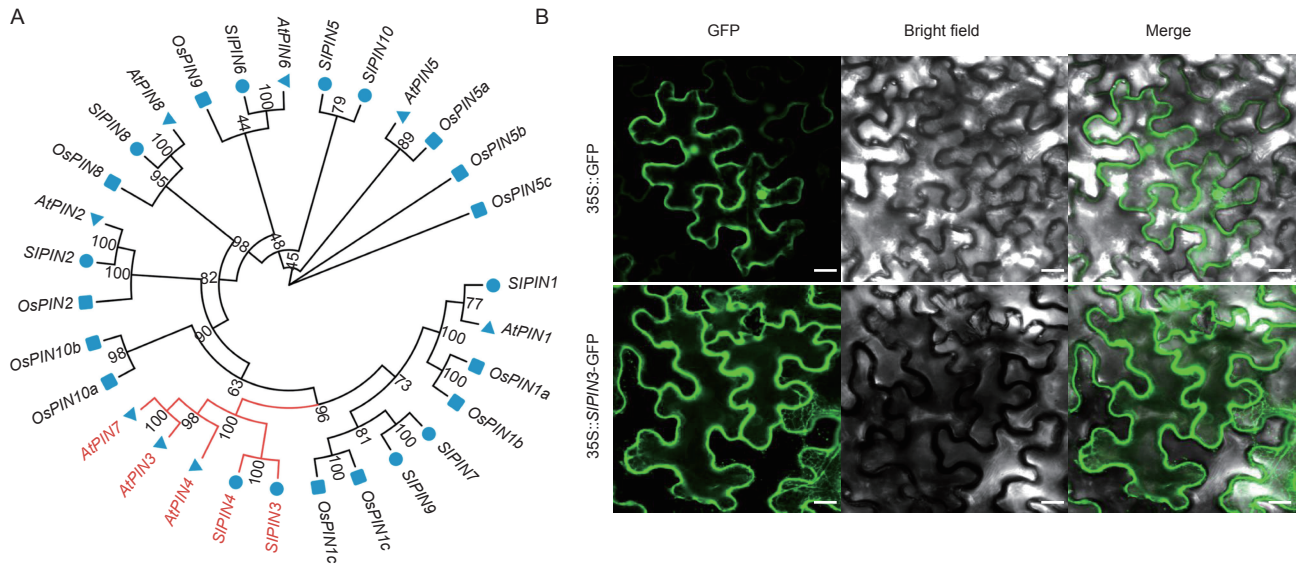



**Fig. 8 Developmental analysis and localization of SlPIN3 protein.** A, evolutionary analysis of the PIN family proteins across *Solanum lycopersicum* L., *Arabidopsis thaliana*, and *Oryza sativa* L. Different species are represented by symbols of various shapes. The protein highlighted in red exhibits a high degree of homology with SlPIN3. B, subcellular localization of 35S::*SlPIN3*-GFP in tobacco. The 35S::GFP construct was utilized as a blank control. Scale bar=20 μm.

was significantly higher than that observed in the NPA environment (Fig. 10-A and C). In the WT, the application of NAA stimulated an increase in *SlPIN3* expression, whereas NPA application inhibited *SlPIN3* expression. In the mutant, *SlPIN3* expression was slightly upregulated following NAA treatment, but remained significantly lower than that of the WT (Fig. 10-B). Furthermore, the expression of *SlPIN3* was nearly undetectable after NPA treatment. In summary, these results indicated that *SlPIN3* played a positive regulatory role in the growth and development of ARs and is involved in the polar transport of auxin.

## 4. Discussion

### 4.1. The induction period of ARs is a crucial phase in their developmental process

Exploring the development mechanisms of ARs significantly enhances the asexual reproduction technology of horticultural crops and enriches the stress resistance network of these plants, ultimately aiding in the creation of superior varieties with robust environmental adaptability (Steffens and Rasmussen 2016). The ARs formed in the hypocotyl of *Arabidopsis* originate from the mesophyll sheath cells of the xylem (Lakehal *et al.* 2020). Omary *et al.* (2022) demonstrated that stem rooting in tomato is initiated by a small group of phloem-related primitive cells. Our observations of the cross-sectional structure of the stem of tomato variety “Y962” revealed that the ARs indeed accumulate root primordia cells near the phloem, corroborating previous findings (Fig. 1-D–I). Despite the differences in the origin of ARs among various plant species, their initiation points exhibit notable similarities, as they are consistently located in the parenchyma cell region adjacent to the vascular cylinder (Bellini *et al.* 2014).

To identify the gene regulatory network involved in the formation of ARs in tomatoes, we selected stem tissues from the “Y962” strain, which produces ARs, and the “W961” strain, which does not. We constructed time-dynamic transcriptomes to analyze these tissues. A significant number of DEGs were identified between the two varieties at various stages of AR development, with the “Y962” strain exhibiting a more pronounced transcriptional variation during the emergence of ARs (Fig. 3-A). This suggests that AR formation is not governed by a single factor; rather, it results from the coordinated action of multiple networks and genes. Statistical analysis of the number of differential genes across different comparison groups revealed that the BD1 comparison group had a higher number of DEGs. Notably, similar findings were also reported in research into AR formation in alfalfa (Ai *et al.* 2023). Thus, we believe that the period of AR induction is a critical phase for the formation of AR primordia and serves as an important regulatory period for gene expression.

### 4.2. Auxin plays a pivotal role in the formation of ARs

Time series analysis of 1,676 overlapping DEGs revealed that the gene sets with the highest transcription levels during AR induction were significantly enriched in the ‘plant hormone signal transduction pathway’ (Fig. 4-B). To further elucidate the expression dynamics and categories of DEGs during AR formation, we performed GO enrichment analysis and GSEA on the overlapping DEGs. Both enrichment methods identified ‘response to auxin’ as the most significantly enriched pathway (Fig. 5-B). This indicates that hormones, particularly auxin, play a crucial role in the initial induction stage of AR formation. Research has demonstrated that the influence of auxin on ARs is not merely a matter of promotion or inhibition; rather, it exhibits a concentration-dependent effect. IAA accumulates at the site of AR formation and facilitates the development

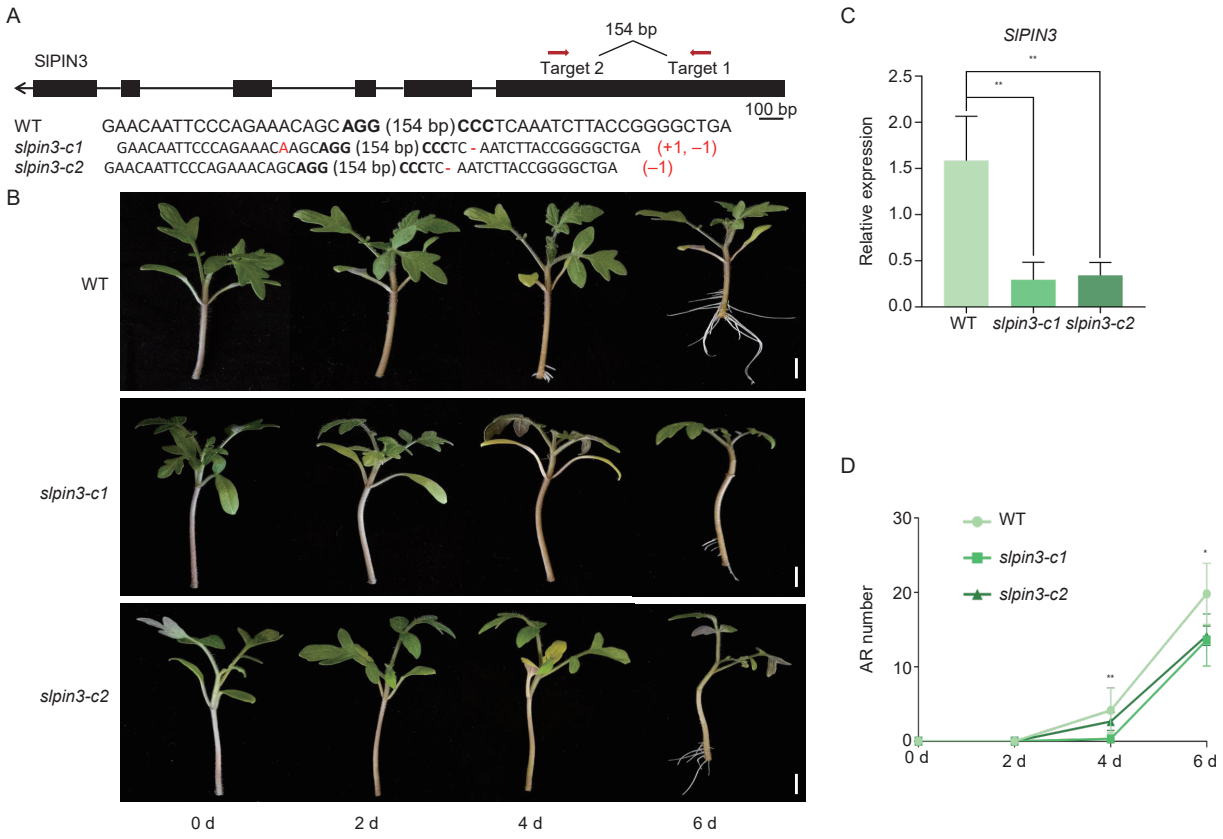



**Fig. 9 Identification and phenotypic analysis of *slpin3* knockout mutants.** A, schematic diagram illustrating the mutation site of the *SlPIN3*. Two sgRNAs were designed for the first exon of *SlPIN3*, referred to as Target 1 and Target 2 (indicated by red arrows). The target site sequence, consisting of 20 bp, is displayed below, with the NGG motif highlighted in bold. Inserted or deleted sequences are marked in red, and the lengths of these sequence gaps are indicated in parentheses. B, observation of the AR phenotype in homozygous mutants *slpin3-c1* and *slpin3-c2*. The main roots of both WT and *slpin3* were excised at 20 d post-germination, and phenotypic changes were documented through photography at 0, 2, 4, and 6 d following hydroponic cultivation. Scale bar=1 cm. C, relative expression levels of *SlPIN3* in WT and *slpin3* mutants. The error bars denote the standard deviation from three biological replicates. Statistical significance was determined using Student's *t*-test, with $^{**}$, $P<0.01$. D, quantification of ARs in WT and *slpin3* mutants. The number of ARs formed at the incision site by WT, *slpin3-c1*, and *slpin3-c2* was recorded at 0, 2, 4, and 6 d. Values are expressed as mean±SE ($n=6$). Statistical significance was assessed using Student's *t*-test, with $^{*}$, $P<0.05$ and $^{**}$, $P<0.01$.

of AR primordia by inducing target cells surrounding the vascular bundle to reprogram in response to rooting stimuli (Klerk *et al.* 1995; Da Costa *et al.* 2013). At the later stages of AR development, high concentrations of auxin inhibit AR elongation, while the root meristem does not require elevated levels of auxins for maintenance once established (Da Costa *et al.* 2013; Verstraeten *et al.* 2014). The determination of free IAA content in the cultivars "W961" and "Y962" revealed that auxin levels peak during the induction stage of AR, confirming that auxin accumulation is a necessary condition for the initiation of AR (Fig. 7-A). Furthermore, our experimental results indicated that the exogenous application of NAA promotes AR growth but inhibits elongation (Fig. 7-B, C and E). This phenomenon may be attributed to the high metabolic stability and low oxidation rate of NAA (De Klerk *et al*. 1999). Any disruption in the biosynthesis, transport, distribution, or signal transduction of auxin can impede the formation of ARs. *AtLAX3* and *AtPIN3* function as auxin influx and efflux carriers during the development of LR primordia. They are induced and expressed by auxin in the early stages of LR formation, with *AtPIN3* being activated first, followed by *AtLAX3* (Péret *et al.* 2013). *AtIAA13*, *AtIAA114*, *AtIAA19*, and *AtIAA29* are recognized as promoting factors for AR formation, while *IAA17* functions as a negative regulator (Fukaki *et al.* 2005; Lakehal *et al.* 2019; Tang *et al.* 2022; Nam *et al.* 2023). *AtSAUR15* and *AtSAUR36* facilitate AR formation through their roles in the auxin signaling pathway (Yin *et al.* 2020; Liu *et al.* 2022). In the comparative group we studied, IAA, LAX, PIN, GH3, and SAUR exhibited significant differential gene expression, with the highest transcriptional abundance recorded during the BD1 stage. The transport and distribution of auxin are essential during the induction phase of ARs (Fig. 6-A).

### 4.3. Interactions between multiple hormones during ARs development

In the development process of ARs, plant hormones play a pivotal role, with their crosstalk contributing to the precision and complexity of AR formation. Cytokinin positively regulates both cell division and root elongation (Riou-Khamlichi *et al*. 1999; Werner *et al*. 2003). Exogenous cytokinin treatment resulted in longer and more numerous

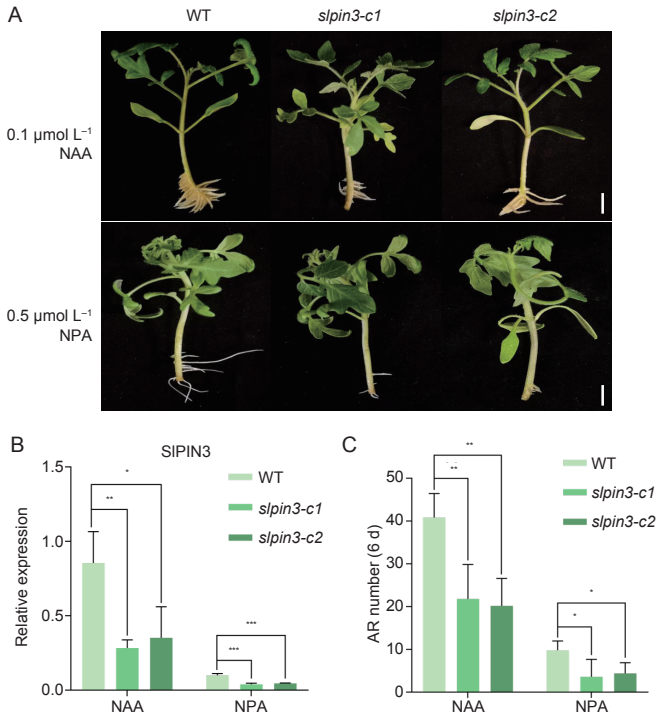



**Fig. 10 *SlPIN3* regulated by exogenous auxin.** A, the formation of ARs in WT and *slpin3* mutants following the exogenous application of 0.1 μmol $L^{-1}$ NAA or 0.5 μmol $L^{-1}$ NPA. Scale bar=1 cm. B, relative expression levels of *SlPIN3* in WT and *slpin3* mutants under treatment conditions with NAA and NPA. C, on the sixth day of treatment, the number of ARs formed at the incision site by WT, *slpin3-c1*, and *slpin3-c2* was counted. Values are expressed as mean±SE ($n$=6). According to Student's $t$-test, $^{*}$, $P$<0.05; $^{**}$, $P$<0.01; $^{***}$, $P$<0.001.

LR in the overexpressed plants RR3 and RR5 compared to the wild type, while *OsRR2* actively regulates crown root initiation (Cheng *et al.* 2010). LOG encodes a cytokinin-inactivating enzyme, and its functional deficiency leads to defects in root development (Tokunaga *et al.* 2012; Satterlee *et al.* 2024). This study found that the A-class ARR genes (*ARR3* and *ARR9*) and LOG genes (*LOG8*, *LOG3*, and *LOG6*) were highly expressed during AR induction, suggesting that they may promote AR formation by enhancing cell differentiation. Gibberellin may serve distinct roles at different stages of AR formation, acting as an inhibitor during the induction phase while promoting development during the formation phase (Guo *et al.* 2012). Additionally, SCR, a member of the GRAS family of transcription factors, is a recognized gene that regulates root differentiation and promotes AR development (Shimotohno *et al.* 2018). Notably, *Solyc05g053090.2* (*SCL14*) exhibited the highest expression level during the BD2 stage, indicating its potential role in the differentiation stage of root primordia. Abscisic acid (ABA) plays a significant role in the development of LRs by antagonizing auxin and cooperating with gibberellin to inhibit the emergence of LRs (Zhang *et al.* 2010). The ABA signal transduction protein PYR/PYL binds to ABA, thereby inhibiting the activity of PP2Cs (Park *et al.* 2009). In this context, the expression levels of *PYL4*, along with *PYL1* and *PYL6*, exhibited a downward trend, while the expression levels of *PP2C* genes showed an upward trend. Notably, the ABA signal transduction pathway is inhibited in the "Y962" genotype, which may, to some extent, weaken the suppression of AR growth. The stimulation of ARs in flooded tomato plants is contingent upon the accumulation of ethylene, which subsequently enhances the transport of plant growth hormones to the flooded site at the stem base, thereby inducing cell division for AR initiation (Negi *et al.* 2010). However, the influence of ethylene on ARs under non-flooded conditions remains contradictory. The expression levels of genes belonging to the ERF class in this study displayed varying trends, suggesting that their impact on ARs warrants further investigation. *TCH4* gene encodes xyloglucan endopeptidase (XET) and is responsive to the brassinosteroid (BRs) signaling pathway. The expression of *TCH4* was exclusively detected in tissues undergoing expansion or modifications of the cell wall (Xu *et al.* 1995). *Solyc07g006860.3*, which encodes XTH, is a homologous gene to TCH4. Based on observed changes in expression, we speculate that BRs may inhibit cell elongation by downregulating the transcription of *TCH4* during the induction phase, while promoting cell elongation by upregulating its expression during the formation phase. *Solyc07g009380.4* (*SlXTH2*) was highly expressed during the induction phase and may play a role in cell division through BRs induction.

### 4.4. Metabolites contribute to the morphogenesis of ARs

The division and differentiation during the formation of ARs require energy input and support from carbon skeletons. The establishment of carbohydrate source pools in roots and stems may induce AR formation (Ahkami *et al.* 2009). Low levels of carbohydrate content can impede the initiation of rooting in cuttings, whereas an increase in sugar content within the rooting medium can accelerate the initiation of ARs (Veierskov *et al.* 1982; Takahashi *et al.* 2003). Our findings indicated that DEGs preferentially expressed in profile 0 during BD1 were enriched in 'starch and sucrose metabolism' (Fig. 4-B), suggesting that sucrose and starch serve as critical carbon sources for energy supply during AR induction, thereby enhancing the metabolic activity of AR primordia and promoting the emergence of ARs. Phenylpropanoids, which are phenolic compounds, play regulatory roles in cell division, differentiation, and metabolism (Cao *et al.* 2020). Among these, flavonoids share similar structures and functions with NPA, which can inhibit the polar transport of auxin (Abas *et al.* 2021). The profile 0 genes, whose expression level consistently declines, were significantly enriched in the phenylpropanoid biosynthesis pathway, while profile 6, which exhibits increased expression in the later stages of AR formation, was significantly enriched in the flavonoid biosynthesis pathway (Fig. 4-B). The key genes involved in flavonoid synthesis, such as *ACO1*, *C4H*, *CHI3*, and *F3H*, demonstrated the lowest expression levels during the BD1 stage in the "Y962" variety, significantly lower than those observed in the MM1 stage of the "W961" variety (Fig. 6-A). We speculate that the low expression

of flavonoid-related genes during the induction period is precisely why endogenous auxin PIN conduction remains largely unaffected, thereby not threatening the initiation of ARs. The elevated expression levels observed during the AR formation period may facilitate the elongation of these roots, as reported by Zhang *et al.* (2021). Expansin protein, a non-enzymatic cell wall-active protein, plays a crucial role in regulating cell wall elongation and relaxation (Lee *et al.* 2003). In this study, we observed significant changes in the expression levels of *LeExpa11*, *ExpaB1*, and *LeExpa4*. Notably, the α-EXPA class genes, *LeExpa11* and *LeExpa4*, exhibited the highest expression levels during the induction period, while the β-EXPB class gene, *ExpaB1*, demonstrated an increase in expression levels during the later stages of AR formation (Fig. 6-A). These transcription results align with the established view that the expression of the expansin protein gene family is adaptable across different organs and tissues, indicating that its function is multifaceted.

### 4.5. *SlPIN3* promotes AR formation by regulating auxin transport

Members of the PIN protein family are integral to the process of auxin efflux, and their asymmetric distribution is crucial for regulating auxin flow, which in turn influences various developmental processes in plants (Vieten *et al.* 2007; Su *et al.* 2022). Based on the length of the hydrophilic ring, PIN proteins are classified into long PINs and short PINs. Long PINs are located on the plasma membrane, whereas short PINs are found on the endoplasmic reticulum (Hu *et al.* 2023). Notably, *SlPIN3* is categorized as a long protein located in the plasma membrane and shares a common ancestor with *AtPIN3* (Fig. 8). The PIN proteins influence the activity of meristematic tissues, the development of elongation zones, and the final morphology of cells by regulating the processes of cell division and elongation. Additionally, phenotypic characteristics such as root length, the number of LRs, and leaf morphology reflect the multifaceted impact of PIN proteins on internal plant development (Blilou *et al.* 2005). During LR development, *AtPIN3* is first transiently expressed in the endothelial layer where the initiating cells emerge, subsequently promoting the transformation of these cells into root primordia. Once the function of *AtPIN3* is impaired, LR germination is inhibited (Péret *et al.* 2013). Based on the hypothesis that *SlPIN3* and *AtPIN3* may have analogous functions, we observed the AR phenotype of tomato with a loss-of-function mutation in *SlPIN3*. The results indicated that the number of ARs in the *slpin3* mutant was significantly lower than that in the WT, and the rate of development was also markedly reduced compared to WT (Fig. 9-B and D). This suggests that *SlPIN3* acts as a positive regulator of AR formation, thereby supporting our hypothesis. The observed defects in AR phenotype may stem from the disruption of PIN polarity distribution, which inhibits the flow and accumulation of auxin, leading to incorrect localization of AR initiation. Furthermore, the application of exogenous auxin not only positively influences the establishment of ARs at the wound site but also induces the expression of PIN genes (Sauer *et al.* 2006). In this experiment, the expression level of *SlPIN3* increased following the addition of NAA but decreased with the application of NPA (Fig. 10-B). In the *slpin3* mutant, although the addition of NAA partially compensated for the loss of *SlPIN3* expression, the number of ARs formed was still significantly lower compared to that in the WT in the absence of NAA (Fig. 10-A and C). These results suggest that auxin accumulation and PIN-mediated polar transport are essential for the normal formation of ARs. NPA inhibits the binding of IAA to PIN3 by interacting with its substrate, thereby serving as an inhibitor of PAT (Su *et al.* 2022). We propose that when the expression of *SlPIN3* is disrupted, the binding interaction between IAA and *SlPIN3* is obstructed, leading to a reduction in the competitive influence of NAA, which is more compatible with *SlPIN3*. Consequently, the ability to inhibit AR formation is enhanced, resulting in a decreased number of ARs.

## 5. Conclusion

In this study, we identified the initiation position and occurrence process of ARs on tomato stems. A transcriptome dataset was established specifically for tomato stem ARs, focusing on the analysis of genes that were significantly differentially expressed in comparison to the induction stage. The results of our research suggest that auxin may serve as a central hub for the comprehensive regulation of various stages of AR formation by integrating other plant hormones. Additionally, the development of ARs is influenced by the metabolic reactions of carbohydrates, flavonoids, and other substances (Fig. 11). *SlPIN3*, a key gene in the auxin transport pathway, plays a positive role in AR formation. When the function of

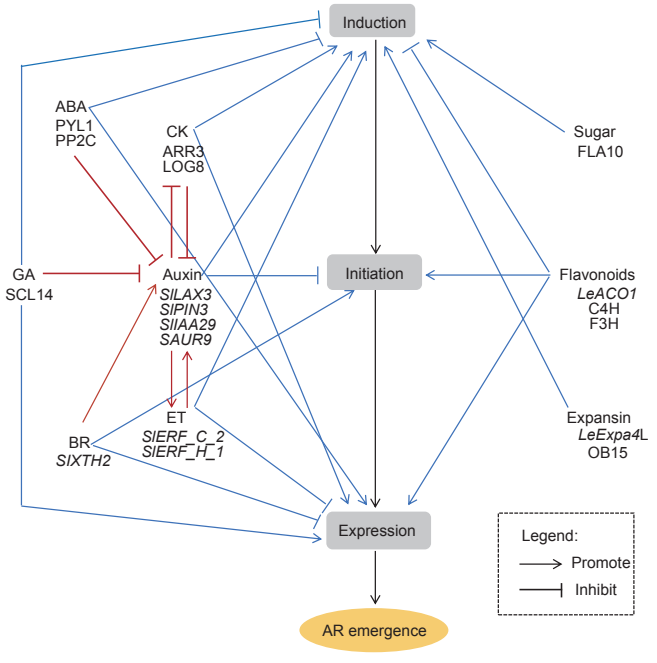



**Fig. 11 A hypothetical model for regulating adventitious root (AR) formation in tomato.** The blue line represents the regulatory effect of plant hormones or metabolites on ARs. The red line represents the crosstalk between auxin and different hormones.

*SlPIN3* is impaired, its mediated polar transport is inhibited, which hinders the normal delivery of auxin and significantly reduces the number of ARs. Our research enriches the regulatory network of tomato ARs and provides new targets for creating AR materials with or without them.

## Acknowledgements

This work was supported by the Natural Science Foundation of Heilongjiang Province, China (LH2024C010 and YQ2024C010), the China Agriculture Research System (CARS-23-A11), and the Special Project of Key R&D Program in Heilongjiang Province, China (SC2022ZX02C0202-01).

## Declaration of competing interest

The authors declare that they have no conflict of interest.

## Declaration of generative AI and AI-assisted technologies in the writing process

The authors declare that they did not use AI in the preparation and writing of this manuscript.

**Appendices** associated with this paper are available at https://doi.org/10.1016/j.jia.2025.12.045

## References

Abas L, Kolb M, Stadlmann J, Janacek D P, Lukic K, Schwechheimer C, Sazanov L A, Mach L, Friml J, Hammes U Z. 2021. Naphthylphthalamic acid associates with and inhibits PIN auxin transporters. *Proceedings of the National Academy of Sciences of the United States of America*, **118**, e2020857118.

Ahkami A H, Lischewski S, Haensch K T, Porfirova S, Hofmann J, Rolletschek H, Melzer M, Franken P, Hause B, Druege U. 2009. Molecular physiology of adventitious root formation in *Petunia hybrida* cuttings: involvement of wound response and primary metabolism. *New Phytologist*, **181**, 613–625.

Ahkami A H, Melzer M, Ghaffari M R, Pollmann S, Ghorbani Javid M, Shahinnia F, Hajirezaei M R, Druege U. 2013. Distribution of indole-3-acetic acid in *Petunia hybrida* shoot tip cuttings and relationship between auxin transport, carbohydrate metabolism and adventitious root formation. *Planta*, **238**, 499–517.

Ai Y, Qian X, Wang X, Chen Y, Zhang T, Chao Y, Zhao Y. 2023. Uncovering early transcriptional regulation during adventitious root formation in *Medicago sativa*. *BMC Plant Biology*, **23**, 176.

Bai T, Dong Z, Zheng X, Song S, Jiao J, Wang M, Song C. 2020. Auxin and its interaction with ethylene control adventitious root formation and development in apple rootstock. *Frontiers in Plant Science*, **11**, 574881.

Bellini C, Pacurar D I, Perrone I. 2014. Adventitious roots and lateral roots: similarities and differences. *Annual Review of Plant Biology*, **65**, 639–666.

Blilou I, Xu J, Wildwater M, Willemsen V, Paponov I, Friml J, Heidstra R, Aida M, Palme K, Scheres B. 2005. The PIN auxin efflux facilitator network controls growth and patterning in *Arabidopsis* roots. *Nature*, **433**, 39–44.

Calvo-Polanco M, Señorans J, Zwiazek J J. 2012. Role of adventitious roots in water relations of tamarack (*Larix laricina*) seedlings exposed to flooding. *BMC Plant Biology*, **12**, 1–9.

Cao B-L, Li N, Xu K. 2020. Crosstalk of phenylpropanoid biosynthesis with hormone signaling in Chinese cabbage is key to counteracting salt stress. *Environmental and Experimental Botany*, **179**, 104209.

Cheng X, Jiang H, Zhang J, Qian Y, Zhu S, Cheng B. 2010. Overexpression of type-A rice response regulators, OsRR3 and OsRR5, results in lower sensitivity to cytokinins. *Genetics and Molecular Research*, **9**, 348–359.

Cheng Y, Dai X, Zhao Y. 2007. Auxin synthesized by the YUCCA flavin monooxygenases is essential for embryogenesis and leaf formation in *Arabidopsis*. *The Plant Cell*, **19**, 2430–2439.

Da Costa C T, De Almeida M R, Ruedell C M, Schwambach J, Maraschin F S, Fett-Neto A G. 2013. When stress and development go hand in hand: main hormonal controls of adventitious rooting in cuttings. *Frontiers in Plant Science*, **4**, 133.

De Klerk G J, Der Krieken, W V, De Jong J C. 1999. The formation of adventitious roots: new concepts, new possibilities. *In Vitro Cellular & Developmental Biology — Plant*, **35**, 189–199.

Debi B R, Taketa S, Ichii M. 2005. Cytokinin inhibits lateral root initiation but stimulates lateral root elongation in rice (*Oryza sativa*). *Journal of Plant Physiology*, **162**, 507–515.

Della Rovere F, Fattorini L, D'angeli S, Veloccia A, Del Duca S, Cai G, Falasca G, Altamura M M. 2015. Arabidopsis SHR and SCR transcription factors and AUX1 auxin influx carrier control the switch between adventitious rooting and xylogenesis *in planta* and in *in vitro* cultured thin cell layers. *Annals of Botany*, **115**, 617–628.

Dharmasiri N, Dharmasiri S, Estelle M. 2005. The F-box protein TIR1 is an auxin receptor. *Nature*, **435**, 441–445.

Ding Z, Galván-Ampudia C S, Demarsy E, Łangowski Ł, Kleine-Vehn J, Fan Y, Morita M T, Tasaka M, Fankhauser C, Offringa R. 2011. Light-mediated polarization of the PIN3 auxin transporter for the phototropic response in *Arabidopsis*. *Nature Cell Biology*, **13**, 447–452.

Franco J, Bañón S, Vicente M, Miralles J, Martínez-Sánchez J. 2011. Root development in horticultural plants grown under abiotic stress conditions-a review. *The Journal of Horticultural Science and Biotechnology*, **86**, 543–556.

Friml J, Palme K. 2002. Polar auxin transport-old questions and new concepts? *Plant Molecular Biology*, **49**, 273–284.

Fukaki H, Nakao Y, Okushima Y, Theologis A, Tasaka M. 2005. Tissue-specific expression of stabilized SOLITARY-ROOT/IAA14 alters lateral root development in Arabidopsis. *The Plant Journal*, **44**, 382–395.

Guan L, Murphy A S, Peer W A, Gan L, Li Y, Cheng Z-M. 2015. Physiological and molecular regulation of adventitious root formation. *Critical Reviews in Plant Sciences*, **34**, 506–521.

Guo D, Liang J, Qiao Y, Yan Y, Li L, Dai Y. 2012. Involvement of G1-to-S transition and AhAUX-dependent auxin transport in abscisic acid-induced inhibition of lateral root primodia initiation in *Arachis hypogaea* L. *Journal of Plant Physiology*, **169**, 1102–1111.

Hu S, Liu X, Xuan W, Mei H, Li J, Chen X, Zhao Z, Zhao Y, Jeyaraj A, Periakaruppan R. 2023. Genome-wide identification and characterization of PIN-FORMED (PIN) and PIN-LIKES (PILS) gene family reveals their role in adventitious root development in tea nodal cutting (*Camellia sinensis*). *International Journal of Biological Macromolecules*, **229**, 791–802.

Inukai Y, Sakamoto T, Ueguchi-Tanaka M, Shibata Y, Gomi K, Umemura I, Hasegawa Y, Ashikari M, Kitano H, Matsuoka M. 2005. *Crown rootless1*, which is essential for crown root formation in rice, is a target of an AUXIN RESPONSE FACTOR in auxin signaling. *The Plant Cell*, **17**, 1387–1396.

Jasik J, De Klerk G J. 1997. Anatomical and ultrastructural examination of adventitious root formation in stem slices of apple. *Biologia Plantarum*, **39**, 79–90.

Kevers C, Hausman J F, Faivre-Rampant O, Evers D, Gaspar T. 1997. Hormonal control of adventitious rooting: progress and questions. *Angew Botanik*, **71**, 71–79.

Klerk G J D, Keppel M, Brugge J T, Meekes H. 1995. Timing of the phases in adventitous root formation in apple microcuttings. *Journal of Experimental Botany*, **46**, 965–972.

Lakehal A, Bellini C. 2019. Control of adventitious root formation: insights into synergistic and antagonistic hormonal interactions. *Physiologia Plantarum*, **165**, 90–100.

Lakehal A, Chaabouni S, Cavel E, Le Hir R, Ranjan A, Raneshan Z, Novák O, Păcurar D I, Perrone I, Jobert F. 2019. A molecular framework for the control of adventitious rooting by TIR1/AFB2-Aux/IAA-dependent auxin signaling in *Arabidopsis*. *Molecular plant*, **12**, 1499–1514.

Lakehal A, Dob A, Rahneshan Z, Novák O, Escamez S, Alallaq S, Strnad M, Tuominen H, Bellini C. 2020. *ETHYLENE RESPONSE FACTOR 115* integrates jasmonate and cytokinin signaling machineries to repress adventitious rooting in *Arabidopsis*. *New Phytologist*, **228**, 1611–1626.

Lee D K, Ahn J H, Song S K, Choi Y D, Lee J S. 2003. Expression of an expansin gene is correlated with root elongation in soybean.

*Plant Physiology*, **131**, 985–997.
Liu R, Wen S S, Sun T T, Wang R, Zuo W T, Yang T, Wang C, Hu J J, Lu M Z, Wang L Q. 2022. PagWOX11/12a positively regulates the *PagSAUR36* gene that enhances adventitious root development in poplar. *Journal of Experimental Botany*, **73**, 7298–7311.
Liu W, Yu J, Ge Y, Qin P, Xu L. 2018. Pivotal role of *LBD16* in root and root-like organ initiation. *Cellular and Molecular Life Sciences*, **75**, 3329–3338.
Mao C, He J, Liu L, Deng Q, Yao X, Liu C, Qiao Y, Li P, Ming F. 2020. OsNAC2 integrates auxin and cytokinin pathways to modulate rice root development. *Plant Biotechnology Journal*, **18**, 429–442.
Mao J, Niu C, Li K, Fan L, Liu Z, Li S, Ma D, Tahir M M, Xing L, Zhao C. 2023. Cytokinin-responsive MdTCP17 interacts with MdWOX11 to repress adventitious root primordium formation in apple rootstocks. *The Plant Cell*, **35**, 1202–1221.
Marhavý P, Vanstraelen M, De Rybel B, Zhaojun D, Bennett M J, Beeckman T, Benková E. 2013. Auxin reflux between the endodermis and pericycle promotes lateral root initiation. *The EMBO Journal*, **32**, 149–158.
Nam H, Han S, Lee S, Nam H, Lim H, Lee G, Cho H S, Dang T V T, Choi S, Lee M M. 2023. CPR5-mediated nucleo-cytoplasmic localization of IAA12 and IAA19 controls lateral root development during abiotic stress. *Proceedings of the National Academy of Sciences of the United States of America*, **120**, e2209781120.
Negi S, Sukumar P, Liu X, Cohen J D, Muday G K. 2010. Genetic dissection of the role of ethylene in regulating auxin-dependent lateral and adventitious root formation in tomato. *The Plant Journal*, **61**, 3–15.
Noh B, Murphy A S, Spalding E P. 2001. *Multidrug resistance*-like genes of Arabidopsis required for auxin transport and auxin-mediated development. *The Plant Cell*, **13**, 2441–2454.
Omary M, Gil-Yarom N, Yahav C, Steiner E, Hendelman A, Efroni I. 2022. A conserved superlocus regulates above-and belowground root initiation. *Science*, **375**, eabf4368.
Park S-Y, Fung P, Nishimura N, Jensen D R, Fujii H, Zhao Y, Lumba S, Santiago J, Rodrigues A, Chow T-F F. 2009. Abscisic acid inhibits type 2C protein phosphatases via the PYR/PYL family of START proteins. *Science*, **324**, 1068–1071.
Péret B, Middleton A M, French A P, Larrieu A, Bishopp A, Njo M, Wells D M, Porco S, Mellor N, Band L R. 2013. Sequential induction of auxin efflux and influx carriers regulates lateral root emergence. *Molecular Systems Biology*, **9**, 699.
Rakusová H, Abbas M, Han H, Song S, Robert H S, Friml J. 2016. Termination of shoot gravitropic responses by auxin feedback on PIN3 polarity. *Current Biology*, **26**, 3026–3032.
Riou-Khamlichi C, Huntley R, Jacqmard A, Murray J A. 1999. Cytokinin activation of *Arabidopsis* cell division through a D-type cyclin. *Science*, **283**, 1541–1544.
Sala K, Malarz K, Barlow P W, Kurczyńska E U. 2017. Distribution of some pectic and arabinogalactan protein epitopes during *Solanum lycopersicum* (L.) adventitious root development. *BMC Plant Biology*, **17**, 1–16.
Satterlee J W, Alonso D, Gramazio P, Jenike K M, He J, Arrones A, Villanueva G, Plazas M, Ramakrishnan S, Benoit M. 2024. Convergent evolution of plant prickles by repeated gene co-option over deep time. *Science*, **385**, eado1663.
Sauer M, Balla J, Luschnig C, Wiśniewska J, Reinöhl V, Friml J, Benková E. 2006. Canalization of auxin flow by Aux/IAA-ARF-dependent feedback regulation of PIN polarity. *Genes & Development*, **20**, 2902–2911.
Shimotohno A, Heidstra R, Blilou I, Scheres B. 2018. Root stem cell niche organizer specification by molecular convergence of PLETHORA and SCARECROW transcription factor modules. *Genes & Development*, **32**, 1085–1100.
Steffens B, Rasmussen A. 2016. The physiology of adventitious roots. *Plant Physiology*, **170**, 603–617.
Su N, Zhu A, Tao X, Ding Z J, Chang S, Ye F, Zhang Y, Zhao C, Chen Q, Wang J. 2022. Structures and mechanisms of the Arabidopsis auxin transporter PIN3. *Nature*, **609**, 616–621.
Sukumar P, Maloney G S, Muday G K. 2013. Localized induction of the ATP-binding cassette B19 auxin transporter enhances adventitious root formation in Arabidopsis. *Plant Physiology*, **162**, 1392–1405.
Takahashi F, Sato-Nara K, Kobayashi K, Suzuki M, Suzuki H. 2003. Sugar-induced adventitious roots in *Arabidopsis* seedlings. *Journal of Plant Research*, **116**, 83–91.
Tang Y, Wang L, Qu Z, Huang C, Zhao T, Li Y, Zhang C. 2022. BSISTER transcription factors directly binds to the promoter of *IAA19* and *IAA29* genes to up-regulate gene expression and promote the root development. *Plant Science*, **321**, 111324.
Tokunaga H, Kojima M, Kuroha T, Ishida T, Sugimoto K, Kiba T, Sakakibara H. 2012. Arabidopsis lonely guy (LOG) multiple mutants reveal a central role of the LOG-dependent pathway in cytokinin activation. *The Plant Journal*, **69**, 355–365.
Veierskov B, Andersen A S, Stummann B, Henningsen K. 1982. Dynamics of extractable carbohydrates in *Pisum sativum*. II. Carbohydrate content and photosynthesis of pea cuttings in relation to irradiance and stock plant temperature and genotype. *Physiologia Plantarum*, **55**, 174–178.
Verstraeten I, Schotte S, Geelen D. 2014. Hypocotyl adventitious root organogenesis differs from lateral root development. *Frontiers in Plant Science*, **5**, 495.
Vidoz M L, Loreti E, Mensuali A, Alpi A, Perata P. 2010. Hormonal interplay during adventitious root formation in flooded tomato plants. *The Plant Journal*, **63**, 551–562.
Vieten A, Sauer M, Brewer P B, Friml J. 2007. Molecular and cellular aspects of auxin-transport-mediated development. *Trends in Plant Science*, **12**, 160–168.
Wang X F, He F F, Ma X X, Mao C Z, Hodgman C, Lu C G, Wu P. 2011. OsCAND1 is required for crown root emergence in rice. *Molecular Plant*, **4**, 289–299.
Wang Z, Yang X, Hu L, Liu W, Feng L, Shen X, Yin Y, Li J. 2024. Transcriptional regulation of *MdPIN7* by MdARF19 during gravity-induced formation of adventitious root GSA in self-rooted apple stock. *Horticultural Plant Journal*, **10**, 1073–1084.
Werner T S, Motyka V, Laucou V, Smets R, Van Onckelen H, SchmüLling T. 2003. Cytokinin-deficient transgenic Arabidopsis plants show multiple developmental alterations indicating opposite functions of cytokinins in the regulation of shoot and root meristem activity. *The Plant Cell*, **15**, 2532–2550.
Wu J, Cheng J, Xu C, Qi S, Sun W, Wu S. 2020. *AUREA* maintains the balance between chlorophyll synthesis and adventitious root formation in tomato. *Horticulture Research*, **7**, 166.
Wu M F, Yamaguchi N, Xiao J, Bargmann B, Estelle M, Sang Y, Wagner D. 2015. Auxin-regulated chromatin switch directs acquisition of flower primordium founder fate. *eLife*, **4**, e09269.
Xie X, Wang Y, Datla R, Ren M. 2021. Auxin and target of rapamycin spatiotemporally regulate root organogenesis. *International Journal of Molecular Sciences*, **22**, 11357.
Xu M, Zhu L, Shou H, Wu P. 2005. A PIN1 family gene, OsPIN1, involved in auxin-dependent adventitious root emergence and tillering in rice. *Plant and Cell Physiology*, **46**, 1674–1681.
Xu W, Purugganan M M, Polisensky D H, Antosiewicz D M, Fry S C, Braam J. 1995. Arabidopsis TCH4, regulated by hormones and the environment, encodes a xyloglucan endotransglycosylase. *The Plant Cell*, **7**, 1555–1567.
Yin H, Li M, Lv M, Hepworth S R, Li D, Ma C, Li J, Wang S M. 2020. SAUR15 promotes lateral and adventitious root development via activating $H^+$-ATPases and auxin biosynthesis. *Plant Physiology*, **184**, 837–851.
Zhang H, Han W, De Smet I, Talboys P, Loya R, Hassan A, Rong H, Jürgens G, Paul Knox J, Wang M H. 2010. ABA promotes quiescence of the quiescent centre and suppresses stem cell differentiation in the Arabidopsis primary root meristem. *The Plant Journal*, **64**, 764–774.
Zhao Y, Cheng S, Song Y, Huang Y, Zhou S, Liu X, Zhou D X. 2015. The interaction between rice ERF3 and WOX11 promotes crown root development by regulating gene expression involved in cytokinin signaling. *The Plant Cell*, **27**, 2469–2483.

Executive Editor-in-Chief Sanwen Huang
Managing Editor Lingyun Weng